The GTPase Rab8 differentially controls the long- and short-range activity of the Hedgehog morphogen gradient by regulating Hedgehog apico-basal distribution

Tanvi Gore, Tamás Matusek, Gisela d'Angelo, Cécile Giordano, Thomas Tognacci, Laurence Lavenant-Staccini, Catherine Rabouille, Pascal Thérond

© 2021. Published by The Company of Biologists Ltd | Development (2021) 148, dev191791. doi:10.1242/dev.191791

RESEARCH ARTICLE

The GTPase Rab8 differentially controls the long- and short-range activity of the Hedgehog morphogen gradient by regulating Hedgehog apico-basal distribution

Tanvi Gore[1,*], Tamás Matusek[1,*], Gisela D'Angelo[1,2], Cécile Giordano[1,2], Thomas Tognacci[1], Laurence Lavenant-Staccini[1], Catherine Rabouille[3,4] and Pascal P. Thérond[1,‡]

ABSTRACT

The Hedgehog (Hh) morphogen gradient is required for patterning during metazoan development, yet the mechanisms involved in Hh apical and basolateral release and how this influences short- and long-range target induction are poorly understood. We found that depletion of the GTPase Rab8 in Hh-producing cells induces an imbalance between the level of apically and laterally released Hh. This leads to non-cell-autonomous differential effects on the expression of Hh target genes, namely an increase in its short-range targets and a concomitant decrease in long-range targets. We further found that Rab8 regulates the endocytosis and apico-basal distribution of Ihog, a transmembrane protein known to bind to Hh and to be crucial for establishment of the Hh gradient. Our data provide new insights into morphogen gradient formation, whereby morphogen activity is functionally distributed between apically and basolaterally secreted pools.

KEY WORDS: Trafficking, Morphogen gradient, Polarized secretion, Rab8, Hedgehog, Interference-of-Hedgehog

INTRODUCTION

Complex intercellular communication is essential for developmental patterning in all metazoans. It depends on both the type of diffusible protein factor and the distance over which they must act. The Hedgehog (Hh) protein family is one of the most enigmatic and atypical signals, and the mechanism of its spreading is highly debated. Understanding how Hh is secreted and spreads is of great importance as defective Hh activity is associated with developmental diseases in humans (Scales and de Sauvage, 2009).

Hh induces the expression of target genes in a concentration-dependent manner. In the *Drosophila* wing imaginal disc, these targets are activated in the anterior (*A*) receiving cells in response to Hh produced in the posterior (*P*) compartment. *A* cells close to the source respond to high levels of Hh by expressing the short-range target transcription factor Engrailed (En) and the Hh receptor Patched (Ptc), which participates in shaping the Hh gradient. *A* cells that are located further away from the source respond to intermediate and low levels of Hh by expressing an intermediate target such as Collier (Col, also known as Knot; Vervoort et al., 1999), and long-range targets such as Decapentaplegic (Dpp), the *Drosophila* homologue of TGFβ (Capdevila and Guerrero, 1994).

The full-length Hh precursor molecule undergoes several post-translational modifications resulting in a functional Hh peptide with a cholesterol moiety attached to its C terminus (Mann and Beachy, 2004) and a palmitic acid on its N terminus (Pepinsky et al., 1998).

Several studies showed that cells release the Hh signal by many different means, including multimers (Gallet et al., 2006; Zeng et al., 2001), lipoprotein particles (Panáková et al., 2005), extracellular vesicles (Gradilla et al., 2014; Matusek et al., 2014; Parchure et al., 2015; Tanaka et al., 2005; Vyas et al., 2014) and long filopodia called cytonemes (Bischoff et al., 2013; Chen et al., 2017; González-Méndez et al., 2017). The molecular machinery mediating the loading of Hh onto these carriers is still poorly understood.

Experimental evidence shows that the Hh gradient might be composed of two pools, an apical and a basolateral one, each linked to the range of Hh activity. Following maturation in the secretory compartments, the dual-lipidated Hh molecule reaches the extracellular leaflet of the apical plasma membrane of the producing cells in *Drosophila* wing imaginal discs (Ayers et al., 2010; Callejo et al., 2011; Gallet et al., 2006). It is then re-internalized, and eventually recycled back to the apical plasma membrane to be released into the extracellular space (D'Angelo et al., 2015). This apically released pool of Hh is thought to activate long-range targets whereas the basolaterally released pool of Hh would activate short-range targets. Accordingly, increasing the amount of extracellular apical Hh or reducing apical spreading of Hh results in the increase and decrease of the Hh long-range activity, respectively (Ayers et al., 2010). In this model, apical and basolateral Hh received in *A* cells depends on two separate apical and basolateral Hh sources from *P* cells.

However, other studies have suggested that Hh is not released apically but predominantly from the basolateral side (Callejo et al., 2011; Bilioni et al., 2013; Chen et al., 2017). In these studies, following endocytosis from the apical membrane, Hh has been proposed to transcytose to the basal pole of *P* cells where it is transported via filopodia and activates short- and long-range targets (Guerrero and Kornberg, 2014). This model proposes that the Hh gradient is composed of a single pool of Hh, which is supplied by a single, indirect route from the basolateral side of *P* cells.

Taken together, this illustrates the controversy regarding the composition of the Hh morphogenetic gradient and the relative contribution of apico-basal trafficking to the regulation of polarized Hh release.

An important factor in the formation of the Hh gradient is the Hh co-receptor Interference-of-Hh (Ihog), a type I transmembrane

[1]Université Côte d'Azur, UMR7277 CNRS, Inserm 1091, Institut de Biologie de Valrose (iBV), Parc Valrose, 06108 Nice cedex2, France. [2]Institut Curie, UMR144 CNRS, 12 Rue Lhomond, 75005 Paris, France. [3]Department of Cell Biology, Hubrecht Institute of the Royal Netherlands Academy of Arts and Sciences & University Medical Center Utrecht, 3584 CT Utrecht, Netherlands. [4]Department of Biomedical Science of Cells and Systems, University Medical Center Groningen, 9700 AD Groningen, Netherlands.
*These authors contributed equally to this work

‡Author for correspondence (therond@unice.fr)

P.P.T., 0000-0003-0434-2334

Handling Editor: Patrick Tam
Received 22 April 2020; Accepted 19 January 2021

Development (2021) 148, dev191791. doi:10.1242/dev.191791

protein necessary for Hh pathway activation (Lum et al., 2003; Yao et al., 2006). Ihog is also expressed in *P* cells and in its absence the association of Hh to apical and basolateral plasma membrane is decreased and Hh is released further (Bilioni et al., 2013; Yan et al., 2010). Its overexpression has also been shown to elevate the level of Hh at the surface of *P* cells, both apically and basolaterally, leading to a restriction of Hh long-range activity (Bilioni et al., 2013; Yan et al., 2010). Taken together, Ihog appears to restrict Hh dispersion after release thereby inhibiting its long-range activity.

In this study, we identify a novel component, Rab8, that is crucial for the proper release of Hh. Rab8 is a monomeric small GTPase that belongs to the Rab8-Rab10-Rab13 subfamily. The *Drosophila* genome contains one conserved Rab8 orthologue sharing 60.4% identity with human RAB8A at the protein level. Rab8 is involved in both endocytic and secretory processes (Hattula et al., 2006; Peränen, 2011; Zhang and Gao, 2016). *Rab8* mutant mammalian cells exhibit increased membrane tension, which slows both endocytic end exocytic processes (Mavor et al., 2016; Vidal-Quadras et al., 2017). In mice, both *Rab8a* and *Rab8a-Rab8b* double mutant intestines display defects in apical cargo deployment with the presence of inclusion bodies, causing microvillus atrophy in enterocytes (Sato et al., 2007, 2014). Rab8 has also been implicated in the basolateral transport of cargoes in mammals and in *Drosophila* (Ang et al., 2003; Henry and Sheff, 2008; Huber et al., 1993; Bellec et al., 2018; Devergne et al., 2017). Moreover, Rab8 has been shown to be necessary for the stabilization of the Rab4-Rab11 recycling compartments in the *Drosophila* neuromuscular junction (West et al., 2015) and also during cellularization during early embryogenesis (Mavor et al., 2016).

Given the role of Rab8 in apico-basal trafficking, it is an ideal candidate for regulation of polarized Hh trafficking and release from *P* cells. Here, we show that interfering with *Rab8* function in *P* cells impedes Hh distribution and target gene expression in *A* cells. The loss of *Rab8* function induces an imbalance between the level of apically and basolaterally released Hh. This results in a reduction of Hh long-range target expression and an increase in the short-range target expression. Mechanistically, loss of *Rab8* function leads to the accumulation of Ihog, especially at the lateral plasma membrane as a result of impairment in Ihog endocytosis. Strikingly, lowering the Ihog level in the *Rab8* mutant rescues the defective short-range target expression. In addition, we show that the loss of *Rab8* induces mispositioning of the early endosomes in which Hh is internalized, which likely contributes to the basolateral increase of released Hh. Our data provides new evidence demonstrating that Hh activity is functionally distributed between apically and laterally secreted pools, each activating long- and short-range targets, respectively.

RESULTS

Loss of *Rab8* function leads to differential defects in Hh target gene expression patterns

To identify new regulators of Hh long-range activity, we performed an RNA interference (RNAi) screen specifically targeting different Rab proteins in *Drosophila*. To monitor Hh long-range activity, we used a 'tester line' in which Hh is specifically and conditionally overexpressed in the posterior compartment (in the same cells as the endogenous Hh). This leads to ectopic expression of the Hh long-range target *dpp* in *A* cells of the wing disc (Matusek et al., 2014; see Materials and Methods), resulting in an outgrowth of the anterior compartment (Matusek et al., 2014; Fig. 1A). To validate the assay, the outgrowth phenotype was rescued by RNAi targeting positive regulators of Hh secretion, including *dispatched* (*disp*; Burke et al., 1999) as well as by removing of one copy of *dpp* or its receptor *tkv* (Fig. 1A). This confirms that this 'tester line' is sensitive to modifications of Hh-dependent *dpp* activity.

Interestingly, depleting *Rab8* led to a significant rescue of *dpp*-dependent anterior outgrowth (a decrease from 95% to 20% of discs showing severe outgrowth is observed upon RNAi against *Rab8*; Fig. 1A). The anterior outgrowth rescue indicates that interfering with Rab8 activity only in *P* cells affects the non-autonomous (long-range) activity of Hh. To confirm this, we analysed the anterior expression of the Hh targets in the tester line. In this context, the increased Hh production in *P* cells induces a substantial expansion of all targets (Fig. 1B-B″), compared with wild-type expression (Fig. 2A-A‴). Although the expansion of En and Ptc stays the same in rescued discs depleted for *Rab8*, the distal expression of *dpp* is decreased (Fig. 1C-F). As the *dpp*-dependent wing disc outgrowth is suppressed, the rescue of anterior outgrowth is unlikely to be due to a change in En and Ptc expression, but due to the decrease of ectopic *dpp* expression.

In order to analyse further the *Rab8* function in Hh secretion, we generated a new loss-of-function allele (see Materials and Methods; Fig. S1A). We recovered one excision that only affected the *Rab8* locus that we named $Rab8^{U1}$ (Fig. S1A). Immunolabelling of wing imaginal discs and western blot analysis on homozygous $Rab8^{U1}$ mutant larval lysate confirmed that the $Rab8^{U1}$ mutant allele is a protein null (Fig. S1B,C). $Rab8^{U1}$ mutant cells displayed no cell polarity defects (Fig. S2A-B‴).

In the absence of Rab8, *dpp* expression is restricted and En expression is broadened

To confirm the role of Rab8 in regulating Hh long-range activity, we analysed the expression of Hh target genes in $Rab8^{U1}$ homozygous mutant wing imaginal discs. As expected, *dpp* expression was severely reduced from a range of six to eight cells in wild type to three to four cells in the $Rab8^{U1}$ mutant (Fig. 2A,A‴,B,B‴,C; Fig. S1D-E). Strikingly, we also observed a change in Hh short-range targets. The anterior expression domain of En was extended to three or four cell rows compared with one or two cell rows in wild type (Fig. 2A′,B′,D) and Ptc expression was mildly extended in $Rab8^{U1}$ mutant tissue (Fig. 2A″,B″,E). The *dpp* phenotype is consistent with a decrease in the long-range activity of Hh, whereas the En phenotype shows an increase in Hh short-range activity. This indicates that *Rab8* loss of function differentially affects Hh targets.

In order to evaluate compartment-specific functions of Rab8, we combined *Rab8* RNAi with a direct protein knockdown system based on deGradFP (see Materials and Methods; Caussinus et al., 2012). Using this technique (referred to as RNAi/deGradFP below), we assessed the function of Rab8 specifically in *P* cells (Fig. S1F,F′). We confirmed that depletion of *Rab8* in *P* cells was not associated with cell death (Fig. S1F″,F‴), or changes in cell architecture (Fig. S2C-D‴). Expansion of En and Ptc was observed in this background too, similar to observations in the $Rab8^{U1}$ mutant (Fig. 2F-H). Expansion of En and Ptc was also observed upon dorsal compartment-specific depletion of *Rab8*, compared with the ventral wild-type pattern (Fig. S1G-H). Neither this expansion nor the change in *dpp* expression was detected when *Rab8* was depleted specifically in *A* cells (Fig. S1I). Importantly, En and *dpp* expression were rescued by re-expressing Rab8 in *P* cells (Fig. S1J-K″), but not in *A* cells (Fig. S1J,L-L″), confirming that the defects observed in Hh target genes are specific to the function of Rab8 in the posterior compartment that produces Hh.

The decrease in distal *dpp* expression is not due to an increased expression of En or Ptc

It is well established that En upregulation leads to suppression of *dpp* transcription (Sanicola et al., 1995). It is therefore possible that the effect of *Rab8* loss is solely due to the broadening of En

Development (2021) 148, dev191791. doi:10.1242/dev.191791

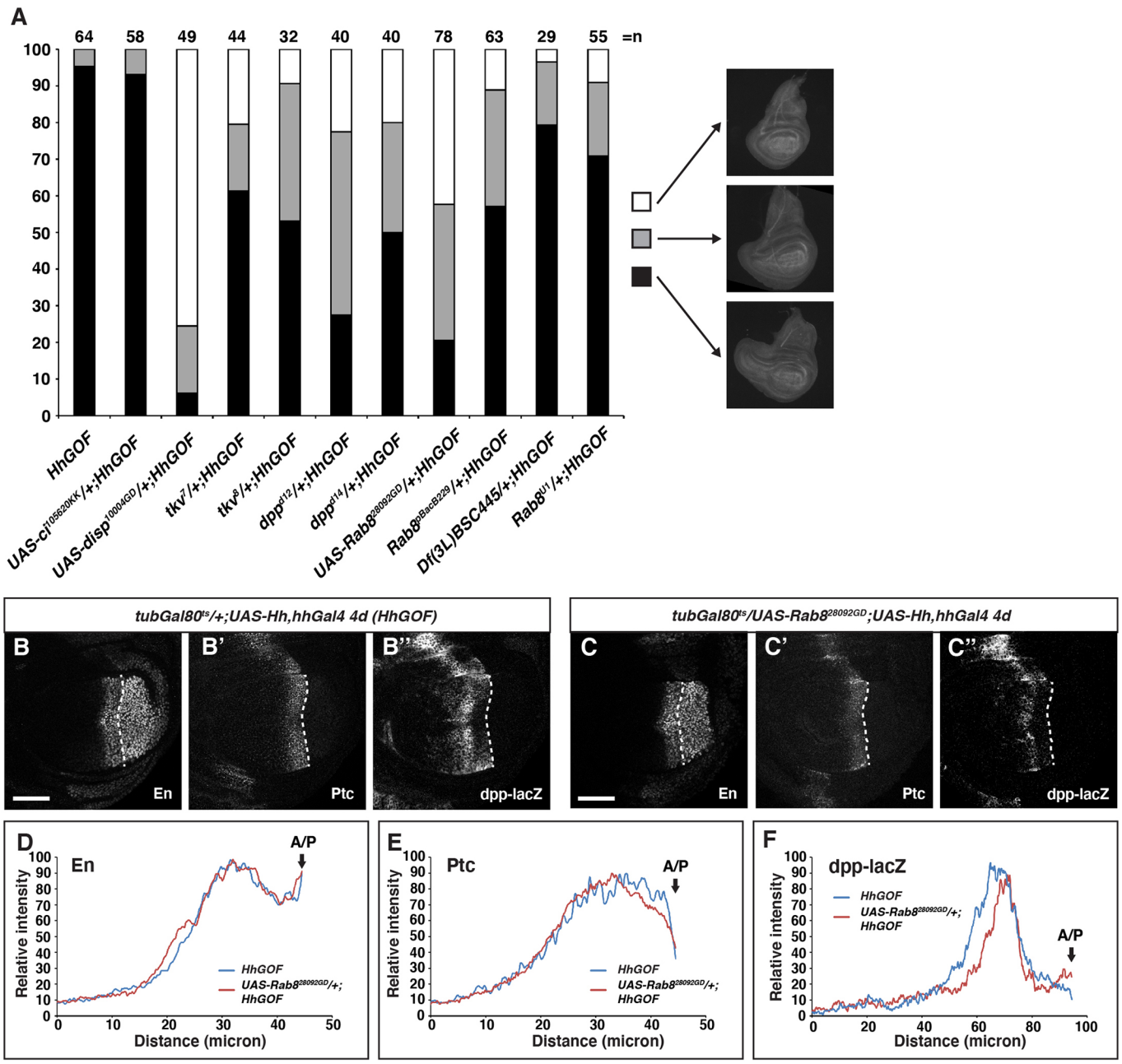

Fig. 1. Interfering with *Rab8* in Hh gain-of-function (HhGOF) condition rescues Hh-dependent anterior outgrowth. (A) Percentage of outgrown, moderately and fully rescued wing discs with respect to their genotypes. The number of dissected discs (*n*) is shown at the top. Representative photographs of each category are shown on the right. Negative UAS control: *ci* RNAi. Positive control: *disp* RNAi. Superscripts refer to the transformant identity of the RNAi lines and alleles. (B-C″) HhGOF control discs (B-B″) and *UAS-Rab8^{28092GD}/+;* HhGOF rescued discs (C-C″) stained with β-gal (*dpp-lacZ*), En and Ptc. In all figures (except when mentioned otherwise) A/P compartment boundaries are marked with white dashed lines, defined by the first *A* cells that express Ptc. Scale bars: 50 µm. Dorsal is up and posterior is to the right. (D-F) Quantification of Engrailed (D, *n*=8), Patched (E, *n*=10) and *dpp-lacZ* (F, *n*=10) in the *A* compartment of HhGOF control discs, and *UAS-Rab8^{28092GD}/+; HhGOF* rescued discs. The A/P boundary is indicated by black arrows.

expression that then restricts *dpp*. However, we found that *dpp* expression is lost not only in *A* cells where En is upregulated but also in the distal *A* cells that do not express En (Fig. 2A,B,C), suggesting that distal *dpp* loss is not coupled to the expansion of En expression. This was also confirmed in the 'tester line', in which the distal expression of *dpp* is decreased, whereas the expression of En and Ptc stays the same in rescued discs depleted for *Rab8* (Fig. 1C-F). To further investigate the link between *dpp* and En expression, we used a strong hypomorphic *hh* mutant combination in which anterior En expression is strongly diminished or absent (see Materials and Methods; Fig. 3A,B,D,G). *A* cells still express *dpp* (with a reduced range; compare Fig. 3A′ with 3B′), which allowed us to test the consequence of depleting *Rab8* on Hh long-range activity independently of En. In this background, depleting *Rab8* exclusively in *P* cells leads to a decrease in distal *dpp* expression (compare Fig. 3A′ and 3C′; quantification in Fig. 3E). Altogether, these data suggest that the loss of distal *dpp* is not solely due to the broadening of anterior En expression.

The decrease in anterior distal *dpp* expression could also be indirectly due to an increased level of Ptc, which could trap released

Development (2021) 148, dev191791. doi:10.1242/dev.191791

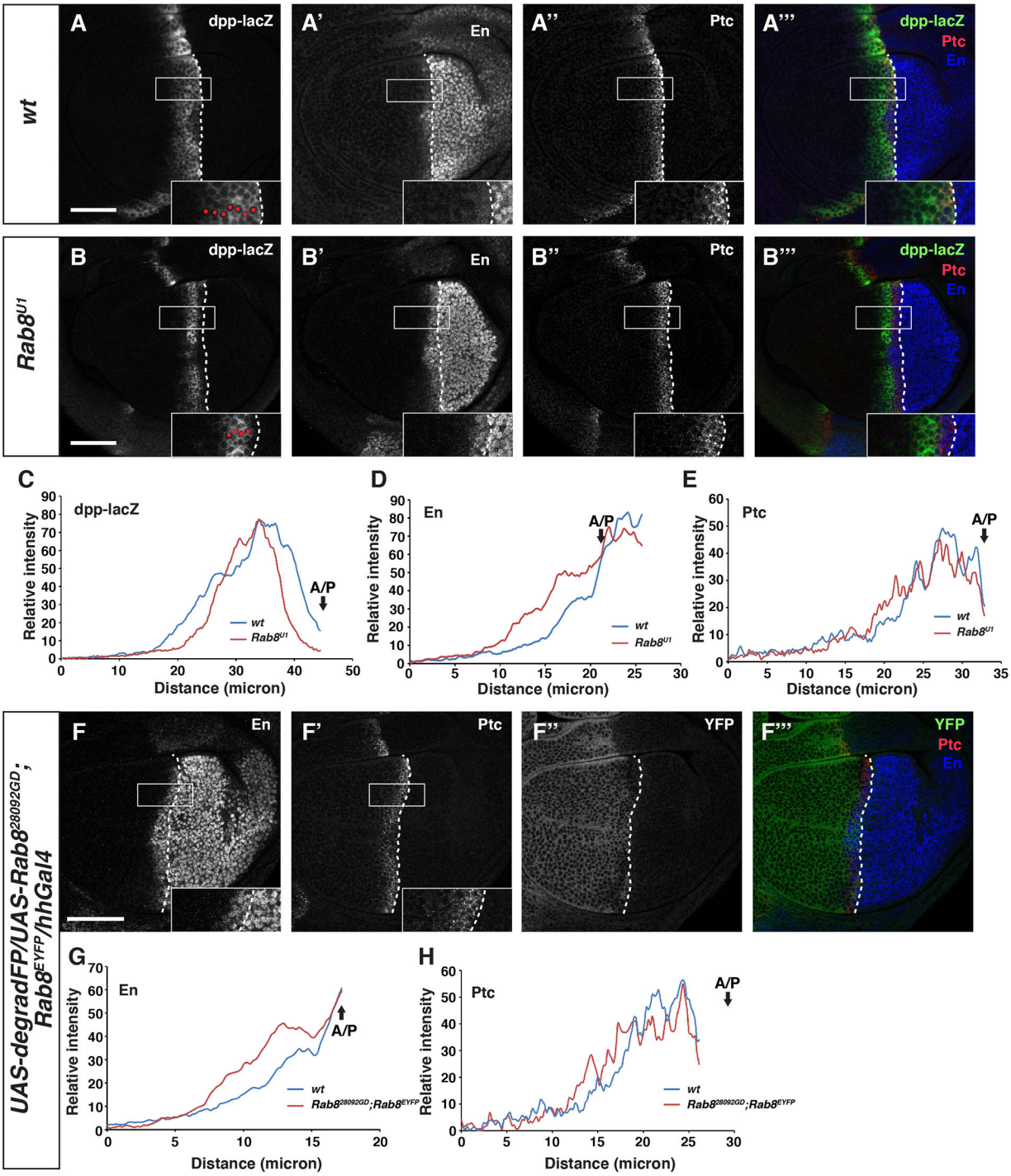

Fig. 2. Loss of *Rab8* function affects both long- and short-range targets of Hh. (A-B‴) Wild-type (wt; A-A‴) and *Rab8^{U1}* mutant (B-B‴) discs stained with β-gal, En and Ptc. Images are single sections of 1 µm thickness, with the exception of A″ and B″, which are *z*-projections of five sections. In all panels, posterior is on the right and dorsal on top. (C-E) Intensity quantification of *dpp-lacZ* (*n*=6), En (*n*=3) and Ptc (*n*=5). (F-F‴) Removal of *Rab8* by the RNAi/deGradFP system in *P* cells. Red dots indicate cells expressing *dpp-lacZ*. Images shown are single sections of 1 µm thickness, with the exception of F′, which is a *z*-projection of five sections. (G,H) Quantification of the data presented in F-F‴ (*n*=7). The A/P boundary in C-E and G,H is indicated by black arrows. White rectangles (A-B‴,F,F′) mark the region shown in the inset of the corresponding panel. Scale bars: 50 µm.

Hh and restrict its spreading to distant *A* cells (Chen and Struhl, 1996). To test this possibility, Ptc domain and level of expression was measured. We found that Ptc level in *A* cells is similar in the presence or absence of posterior Rab8 in this setting (Fig. 3A″,B″, C″,F,H) strongly suggesting that the decreased *dpp* expression is not indirectly due to an increased level of Ptc.

Lastly, we confirmed that the rescue of wing disc outgrowth was not due to impaired maturation of the Hh precursor molecule as Hh cleavage is not affected in the *Rab8* mutant (Fig. S3A).

These results reveal a positive contribution of Rab8 within *P* cells to long-range activity of Hh that is independent of both Ptc levels and En expression. Altogether, our results show that depletion of

Development (2021) 148, dev191791. doi:10.1242/dev.191791

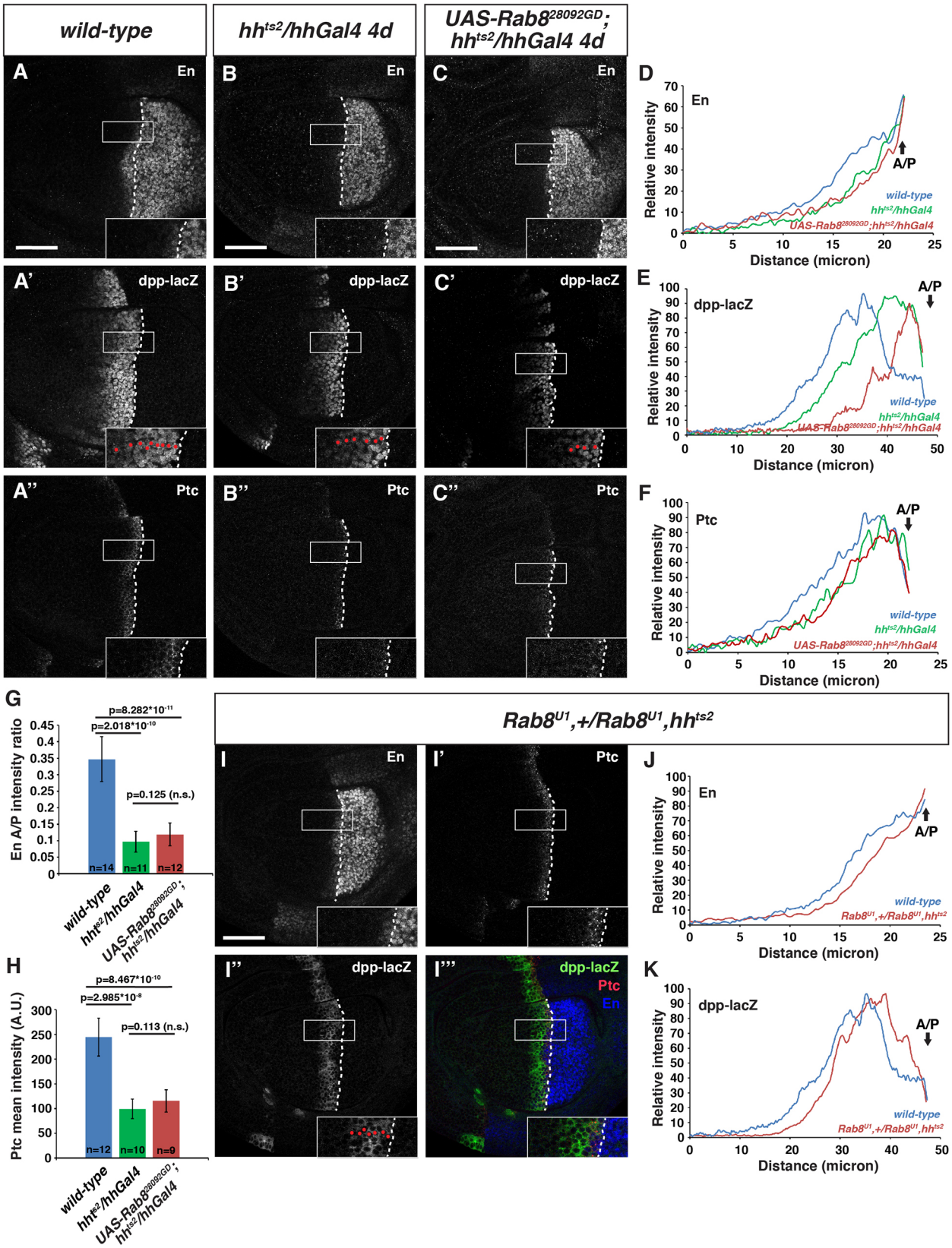

Fig. 3. *Rab8* loss of function induces a decrease in long-range Hh target gene expression. (A-C″) Wild-type discs (A-A″), hh^{ts2}/*hhGal4* hypomorph discs (B-B″) and hh^{ts2}/*hhGal4* discs expressing *Rab8* dsRNA in *P* cells (C-C″) stained with En, *dpp-lacZ* and Ptc. (D-F) Quantification of En (n=4), *dpp-lacZ* (n=9) and Ptc (n=4) range presented in A-C″. (G,H) Quantification of En (G) and Ptc (H) intensities in the genotypes presented in A-C″. A.U., arbitrary unit; n.s., not significant. (I-I‴) $Rab8^{U1}$,+/$Rab8^{U1}$,hh^{ts2} disc stained with En, *dpp-lacZ* and Ptc. (J,K) Quantification of En (J) and *dpp-lacZ* (K) intensities in $Rab8^{U1}$,+/$Rab8^{U1}$,hh^{ts2} discs (n=10). In A-C″ and I-I‴ dorsal is up and posterior is to the right. The A/P boundary in D-F and J,K is indicated by black arrows. The white rectangles mark the regions shown in the insets. Red dots indicate cells expressing *dpp-lacZ*. Scale bars: 50 µm.

Development (2021) 148, dev191791. doi:10.1242/dev.191791

Rab8 specifically in *P* cells leads to differential defects in the Hh gradient, leading to a decrease in long-range and an increase in short-range activity.

Rab8 function is required for proper apico-basolateral distribution of Hh

The differential changes in target gene expression observed in $Rab8^{U1}$ homozygotes (Fig. 2) prompted us to determine whether Hh is abnormally released from *Rab8* mutant *P* cells. Using western blot analysis from $Rab8^{U1}$ homozygote larvae overexpressing Hh in *P* cells, we did not detect any change in the level of overexpressed Hh compared with the control (Fig. S3A).

We also quantified Hh release from non-polarized Schneider-2 (S2) cells using Hh-*Renilla* (Hh-Ren), a reporter of Hh secretion (Aikin et al., 2012). Hh-Ren is secreted, biologically active, and detected at a similar level in the medium of wild-type and *Rab8* dsRNA-treated S2 cells (Fig. S3B). These data suggest that the *Rab8* mutant phenotype is not due to an overall change in the level of Hh production or release.

Imbalance between apically and laterally released Hh in a *Rab8* loss-of-function context

Given the proposed relationship between short- and long-range Hh targets and the relative contribution of apico-basolaterally released Hh (see Introduction), we hypothesized that there could be an imbalance in the apical-basal ratio of released Hh. To investigate this, we used a strategy in which released Hh gets 'trapped' in *A* cells, by overexpressing a mutant form of Ptc receptor (Ptc^{1130X}; Johnson et al., 2000) that is deficient for endocytosis. It has been previously shown that extracellular Hh binds Ptc^{1130X}, which sequesters it at the plasma membrane but prevents its internalization. We first expressed Ptc^{1130X} throughout development (see Materials and Methods) and found trapped Hh throughout the apico-basal axis in Hh-receiving *A* cells (Fig. 4A-A‴, fixed tissue with detergent). Hh appeared to accumulate more at the apical side of the *A* cells. In the $Rab8^{U1}$ mutant, however, this apical accumulation was not observed, but Hh accumulation laterally was still present (Fig. 4B-B‴).

In order to confirm these data, we reduced the duration of Ptc^{1130X} induction to 4 h and analysed Hh distribution on fixed tissue without detergent (extracellular Hh; ExHh). In control tissue, apical and lateral trapping of ExHh was observed in *A* cells (Fig. 4C,D,G,H-H‴). The distribution of ExHh in *P* cells was relatively uniform along the apico-basal axis (Fig. 4G′). In the $Rab8^{U1}$ mutant, we observed a decreased apical and increased lateral trapping of ExHh in *A* cells (Fig. 4E,F,G,I-I‴). Interestingly, we also found a lateral increase of ExHh in *P* cells (Fig. 4G′). In contrast to our observations in *A* cells, we measured a slight increase in apical Hh in *P* cells (Fig. 4G′,I). This increase was not correlated with an increase of apically released Hh in *A* cells, suggesting that apical Hh release from *P* cells is reduced. Notably, overall Ptc distribution along the apico-basal axis was not affected by *Rab8* loss of function (Fig. 4A′,B′,H′,I′; Fig. S4A-D′). A scheme of the quantification method used to measure Hh bound to Ptc^{1130X} is presented in Fig. S4E.

Taken together, our data indicate that the $Rab8^{U1}$ phenotype might be due to the amount of released Hh that is abnormally present at the lateral side of receiving *A* cells. We propose that this is a consequence of an increase of laterally released Hh from *P* cells at the expense of its apical release (Fig. 4G′). This, in turn, promotes high level, short-range Hh signalling in *A* cells. In conclusion, our data suggest that Rab8 plays an important role in ensuring the balanced apico/basal distribution of released Hh.

Reduction of Hh level rescues the increased short-range activity observed in the *Rab8* mutant

To test if the *Rab8* mutant phenotype is due to an increase in basolaterally released Hh, we removed one copy of *hh* in a $Rab8^{U1}$ mutant background (hh^{ts2}<$Rab8^{U1}$/$Rab8^{U1}$). If the $Rab8^{U1}$ phenotype was due to an increase in released Hh, we reasoned that decreasing the overall level of Hh would reduce the amount of Hh below the threshold required to activate En expression, therefore suppressing the proximal loss of *dpp-lacZ* expression in this genotype. Strikingly, En expression was strongly diminished and proximal *dpp* expression was restored, suggesting that the elevated level of released Hh at the basolateral side is responsible for the Rab8-dependent defects in proximal Hh signalling (Fig. 3I-K). Of note, in this experiment, we did not expect a rescue of distal *dpp* expression as we further reduced the overall level of Hh including the pool that is released apically.

Rab8 is required for Ihog endocytosis

To address how Rab8 mediates the balance of apico-basal Hh release, we investigated its role in the subcellular distribution of the endogenous Ihog, which is known to play a role in the basolateral release of Hh (see Introduction).

We directly compared wild-type and *Rab8* mutant cells in the same tissue, by using the RNAi/deGradFP system with the dorsal compartment-specific *apGal4* driver (therefore the ventral compartment served as an internal control; Fig. 5A). Here, we observed consistently a stronger Ihog signal mainly at the lateral plasma membrane in the *Rab8*-depleted compartment than in its wild-type counterpart (Fig. 5A′; quantification section by section in Fig. 5B and Fig. S5A,B). To confirm this, we analysed Ihog in non-prefixed tissue without detergent, which reveals the presence of the protein at the cell surface. We observed again an increase of Ihog (by 2-fold) at the lateral side of the cells (Fig. 5C-D′; quantification in Fig. S5C,D).

These results indicate that Rab8 is required for the correct apico-basal distribution of the Hh co-receptor Ihog at the plasma membrane.

In the *Rab8* mutant, plasma membrane Ihog is more stable

One possible explanation for the accumulation of Ihog at the lateral membrane of *Rab8* mutant cells is that it is endocytosed to a lesser extent and becomes stabilized at the plasma membrane. To test this, we measured the stability of overexpressed IhogRFP at the plasma membrane in wild-type and $Rab8^{U1}$ mutant discs. To do so, IhogRFP was overexpressed in *P* cells during a 1-day pulse (Fig. 5E-F′), and the decrease of IhogRFP fluorescence was monitored after 3 days during which its production was stopped (see Materials and Methods). In wild-type discs, IhogRFP was efficiently removed after 3 days and its level was low (Fig. 5G,G′), suggesting an efficient turnover through endocytosis. In $Rab8^{U1}$ mutant tissue, however, IhogRFP was less efficiently removed from the plasma membrane, particularly at the lateral side, consistent with an impairment of Ihog endocytosis (Fig. 5H,H′). Of note, we can rule out an increased delivery of newly synthesized Ihog replenishing the basolateral plasma membrane, because the level of Ihog at day 1 was the same for both backgrounds (Fig. 5E-F′) and the synthesis of IhogRFP was subsequently stopped.

Taken together, these results suggest that Ihog is more stable at the plasma membrane of *Rab8* mutant cells. This is consistent with efficient Ihog internalization in wild-type discs that is impaired in the absence of *Rab8* function.

In the *Rab8* mutant, endocytosis of Ihog is decreased

To confirm that Rab8 regulates endocytosis of Ihog, we designed an assay to monitor the localization of endogenous Ihog in the

Development (2021) 148, dev191791. doi:10.1242/dev.191791

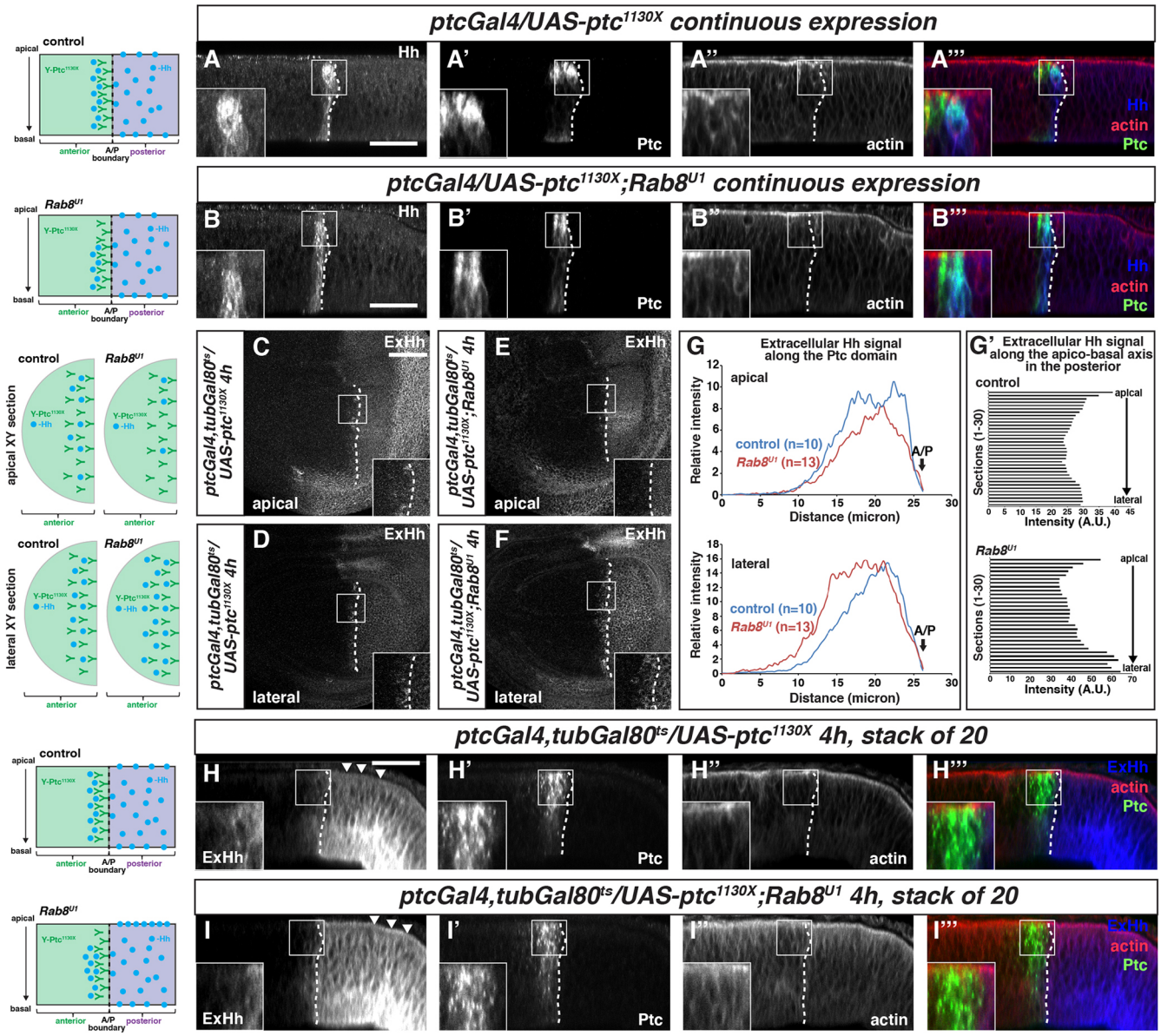

Fig. 4. Removal of *Rab8* function leads to abnormal distribution of released Hh. (A-B‴) Hh, Ptc and actin localization after continuous expression of Ptc^{1130X} in *A* cells in wild type (A-A‴) and *Rab8^{U1}* mutant (B-B‴). (C-I‴) Hh (extracellular, ExHh), Ptc and actin localization after expression of Ptc^{1130X} for 4 h in *A* cells in wild type and *Rab8^{U1}* mutant. (G,G′) Quantification of extracellular Hh in *A* cells (G) and *P* cells (G′) in wild-type and *Rab8^{U1}* mutant discs expressing Ptc^{1130X}, at different levels from apical to lateral, on multiple disc samples. The A/P boundary in G is indicated by black arrows. White arrowheads in H,I indicate the difference between apical Hh levels in *P* cells. White squares in A-B‴, C-F and H-I‴ mark the region shown in the insets. In C-F dorsal is up and posterior is to the right. In A-B‴ and H-I‴ apical is up and posterior is to the right. A-B‴ and C-F are stacks of three sections of 1 µm thickness. Discs were fixed with (A-B‴), or without (C-F,H-I‴) detergent. Schematics of the presented data are to the left of the panels. Scale bars: 50 µm.

endosomal pathway. First, we overexpressed a constitutively active form of Rab5 (Rab5^{CA}-YFP) in dorsal cells, encompassing both Hh-producing and -receiving cells. Note, that Rab5^{CA} and the Rab5 knock-in (Rab5^{KI}) variants show a similar distribution with strong enrichment at the apical and subapical domains (Fig. S6A-C). We then monitored the presence of endogenous Ihog in the Rab5^{CA}-YFP-labelled early endocytic structures (Fig. 6A-C‴). Here, numerous apical Rab5^{CA}-YFP endosomes were positive for Ihog protein (Fig. 6A,A′,B,B′,C,C′); however, they were not positive for Rab8 (Fig. 6A″,B″,C″). Moreover, in very distal *A* cells, which express a very low level of Ptc and do not respond to Hh, we also found Rab5^{CA}-YFP endosomes positive for Ihog (Fig. 6A‴, far left). This experiment reveals that in both *A* and *P* cells, endogenous Ihog is endocytosed at least to early endosomes and that this endocytosis could be independent of Hh and Ptc.

We then investigated whether the distribution of Ihog in endosomes was modulated by Rab8. In the *Rab8^{U1}* mutant, the number of Rab5^{CA}-YFP-positive structures was essentially the same as in control, but we noticed that they were no longer apical. Instead, compared with the control (Fig. 7A,B,C,G; Fig. S6D-F″), the percentage of the most apical Rab5^{CA}-YFP endosomes changed significantly from 53% to 30% in *Rab8^{U1}* homozygous tissue (Fig. 7D,E,F,G; Fig. S6G-I″). We observed a similar trend with Rab5^{KI} distribution in the *Rab8* mutant. The percentage of apical/subapical endosomes decreased from 70% to

Development (2021) 148, dev191791. doi:10.1242/dev.191791

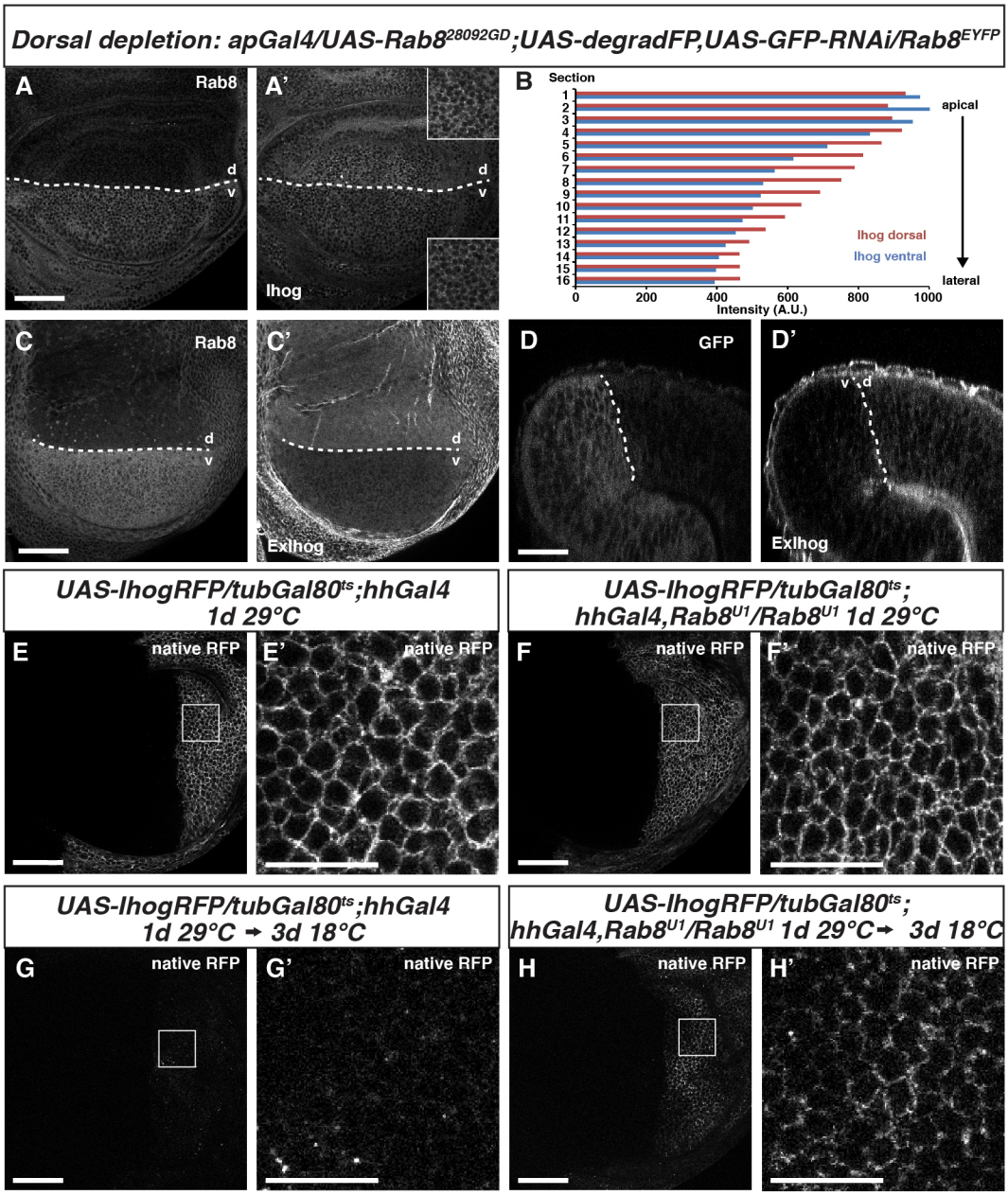

Fig. 5. *Rab8* loss of function results in impaired apico-basal distribution of Ihog. (A-D′) Ihog subcellular (A-B) and extracellular (C-D′) distribution in discs in which *Rab8* function has been removed by the RNAi/deGradFP system (A) in exclusively dorsal cells. In A′ the insets show magnification of Ihog immunolabelling from the dorsal (d) and ventral (v) posterior tissues, respectively. (B) Quantification of Ihog at different *xy* levels from apical to lateral, section by section, on a representative sample. The white dashed lines in A,A′ and C-D′ mark the dorsoventral boundary defined by the lack of Rab8 (A,C) or GFP (D) labelling. (E-F′) IhogRFP fluorescence after 1 day pulse in the *P* compartment in wild type (E,E′) or in *Rab8* mutant (F,F′). (G-H′) IhogRFP fluorescence in control (G,G′) and *Rab8* mutant (H,H′) after 3 days chase. E′,F′,G′,H′ show magnifications of the boxed areas in E,F,G,H. In *xy* sections dorsal is up, posterior is to the right. Scale bars: 50 µm.

40%, with 60% of endosomes now located below the 5 µm mark from the apical marker (Fig. S6J-K).

Taken together, Rab8 is required for the apical positioning of Rab5 endosomes. We also noticed that only 14% of Rab5^{CA}-YFP positive endosomes were positive for Ihog in the *Rab8* mutant background (versus 29% in the wild-type control, Fig. S6L), showing that loss of Rab8 impairs Ihog trafficking to these early endosomes.

These results suggest that in the wild-type context, endogenous Ihog is present at the plasma membrane and is efficiently endocytosed. However, in the *Rab8* loss-of-function context, the level of Ihog at the plasma membrane increases because the protein is not efficiently endocytosed and therefore accumulates.

Given the effect of *Rab8* loss of function on Ihog dynamics, we asked whether Ihog and Rab8 interact at the protein level. To address this question, we co-transfected S2 cells with Ihog-HA and Rab8-YFP (Fig. 6D), and observed that Ihog and Rab8 co-precipitate. Using different Ihog variants, we confirmed this result, and found that the C-terminal cytoplasmic domain of Ihog is required for this interaction (Fig. 6E). This result strongly suggests that Rab8 influences Ihog internalization through protein-protein interaction.

Development (2021) 148, dev191791. doi:10.1242/dev.191791

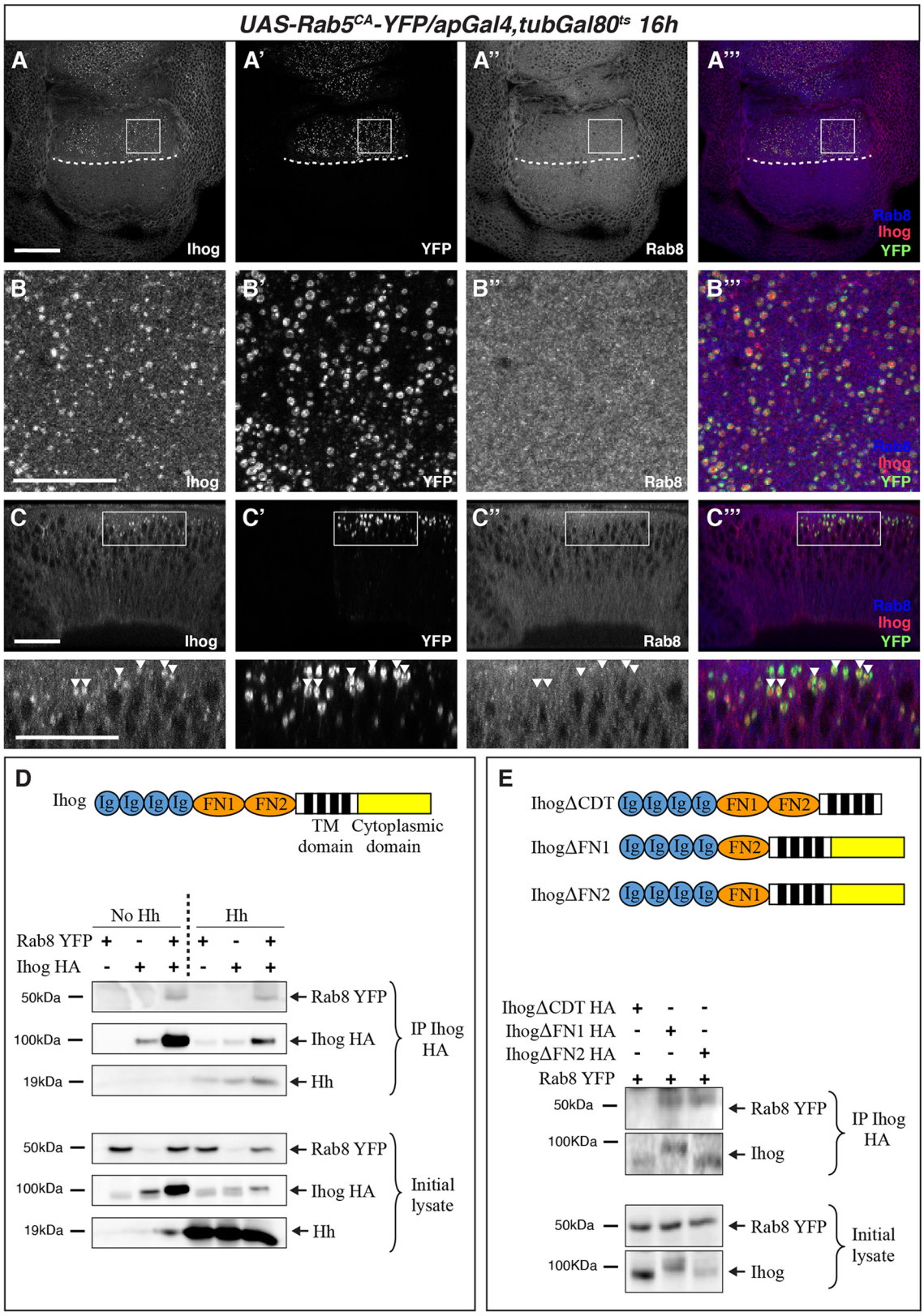

Fig. 6. Presence of Ihog in Rab5^{CA}-YFP -positive endosomes and interaction between Ihog and Rab8. (A-B‴) Overexpression of Rab5^{CA}-YFP in the dorsal compartment of a wild-type disc. (C-C‴) The same experiment showing a posterior single *z*-section. White arrowheads mark vesicles containing Ihog but not Rab8. The white rectangles in A-A‴ and C-C‴ mark the part of the magnified images displayed in B-B‴ and C-C‴, respectively. In A-B‴ dorsal is up and posterior is to the right. In C-C‴ apical is up and dorsal is to the right. The white dashed lines in A-A‴ mark the dorsoventral boundary defined by the Rab5^{CA}-YFP signal. Scale bars: 50 µm. (D) Rab8 is found in one immunocomplex with Ihog. (E) Rab8-Ihog interaction is dependent on the Ihog C-terminal cytoplasmic domain. FN1 and FN2, fibronectin domains 1 and 2; Ig, immunoglobulin-domain; TM, transmembrane domain.

Development (2021) 148, dev191791. doi:10.1242/dev.191791

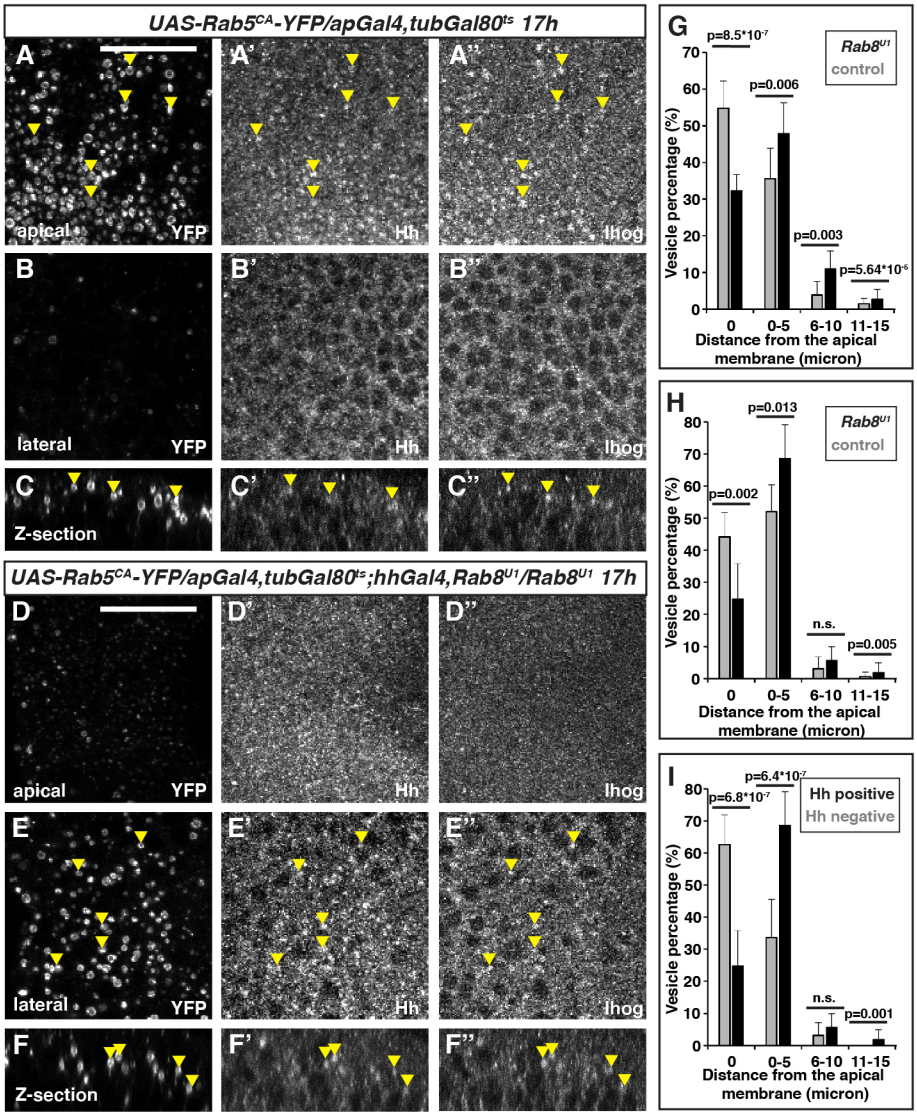

Fig. 7. Hh- and Ihog-containing Rab5^{CA}-YFP endosomes are mislocalized in *Rab8* mutant tissue. (A-C″) Overexpression of Rab5^{CA}-YFP in Hh-secreting cells. A-B″ show *xy* apical (A-A″) and lateral (B-B″) sections (of 1 µm thickness) and C-C″ show corresponding single posterior *z*-sections with apical up. (D-F″) Overexpression of Rab5^{CA}-YFP in Hh-secreting cells in the *Rab8^{U1}* mutant. D-E″ show *xy* apical (D-D″) and lateral (E-E″) sections (of 1 µm thickness) in posterior cells. F-F″ show corresponding single *z*-sections with apical up. Yellow arrowheads mark Rab5^{CA}-YFP-positive vesicles containing both Hh and Ihog. Scale bars: 50 µm. (G) Rab5^{CA}-YFP vesicle distribution in control (*n*=313) and *Rab8^{U1}* mutant (*n*=376) discs. (H) Hh-containing Rab5^{CA}-YFP vesicle distribution in control (*n*=159) and *Rab8^{U1}* mutant (*n*=104) discs. (I) Hh-negative (*n*=135) and Hh-positive (*n*=104) Rab5^{CA}-YFP vesicle distribution in *Rab8^{U1}* mutant discs. n.s., not significant.

Internalized Ihog is not degraded in wild-type discs

The Ihog accumulation observed in *Rab8^{U1}* mutant cells could also imply that Ihog degradation might be compromised in *Rab8* mutant cells. To evaluate the extent of this possible lysosomal-dependent degradation of Ihog, we generated clones of cells mutant for *deep orange* (*dor*), which encodes a homologue of the yeast VPS18 protein that is required for the fusion of endosome to lysosomes, hence delivering endocytosed cargo for degradation (Sevrioukov et al., 1999). *dor* loss of function resulted in the accumulation of poly-ubiquitylated epitopes (poly-Ubi) of these endocytosed cargos to degradative lysosomes (Fig. S7A-A″). However, Ihog did not appear to accumulate in lysosomes, suggesting that internalized endogenous Ihog is not targeted to degradation in this compartment (Fig. S7B-C″). We also induced the expression of a dominant-negative form of the ESCRTIII protein Vps4 (Vps4^{DN}; Babst et al., 1997; Fujita et al., 2003; Rusten et al., 2007) in *P* cells, which induces the formation of maturation-deficient endosomes. As above, intracellular endogenous Ihog was not trapped in these structures, whereas HRS, a member of the ESCRT0 complex, was trapped (Fig. S7D-E″). We therefore conclude that, following its endocytosis, internalized Ihog is not degraded in the lysosomes of the *P* cells.

Rab8 function on Ihog is not influenced by Hh

As Ihog and Hh are also known to bind each other, we tested whether Rab8/Ihog interaction was modulated by Hh. We performed the pulldown in the absence or presence of Hh, but Hh does not change this interaction (Fig. 6D). However, the binding of Rab8 and Ihog, the strong *hh* phenotype resulting from *Rab8* loss of function combined with the fact that Hh is also internalized in the *P* cells as described (D′Angelo et al., 2015) prompted us to analyse whether the role of Rab8 in Ihog endocytosis is modulated by Hh. We began by asking whether in wild-type discs the Ihog endocytic compartment is the same early apical Rab5-positive endocytic compartment through which Hh traffics. To investigate this, we looked for the co-presence of Ihog and Hh in Rab5^{CA}-YFP endocytic structures in *P* cells (Fig. 7A-C″; Fig. S6D-F″; for details, see Materials and Methods). We found that 29% of the Rab5^{CA}-YFP endosomes were positive for Ihog, 28% contained only Hh, and 13% were labelled by both Hh and Ihog (Fig. S6L). These results suggest that Ihog and Hh can be endocytosed independently of one another but that they can also be trafficked through the same endosomes probably because they bind to each other at the plasma membrane.

We then asked whether Ihog and Hh co-distribution was modulated by Rab8. As mentioned above, only 14% of Rab5^{CA}-

Development (2021) 148, dev191791. doi:10.1242/dev.191791

YFP-positive endosomes were positive for Ihog in the $Rab8^{U1}$ mutant. However, the same percentage of endosomes positive for both Ihog and Hh was found as in the wild type (12% versus 13%) and the number of endosomes only positive for Hh was only slightly reduced compared with wild type (23% versus 28%) (Fig. 7D-F″; Fig. S6G-I″,L).

Of note, the analysis of Hh-containing $Rab5^{CA}$-YFP endosomes in control and *Rab8* mutant background showed a distribution trend similar to that observed for $Rab5^{CA}$-YFP, with a change of the percentage of the most apical Hh endosomes from 43% to 23% in $Rab8^{U1}$ homozygous tissue (Fig. 7H). This is associated with more than 65% of Hh endosomes being located in a more lateral position. Surprisingly, the endosomes containing Hh do not behave similarly to those without Hh. In the *Rab8* mutant, the percentage of apical Hh-positive endosomes is one-third of the percentage of apical Hh negative endosomes, suggesting that Hh-containing endosomes tend to localize more towards the lateral side (Fig. 7I). This suggests that in the *Rab8* mutant Hh is likely more efficiently recycled at the lateral side at the expense of the apical.

We conclude that Rab8 is involved in the internalization of free Ihog (the pool of Ihog that does not bind Hh; Fig. S6L) resulting in its increased accumulation/stabilization at the lateral plasma membrane. Of note, elevated Ihog level (by IhogRFP overexpression in wild-type Hh-secreting cells) at the plasma membrane does not lead to Rab5 endosome mislocalization (Fig. S6M-M″). Absence of *Rab8* does not influence the internalization of the Ihog/Hh complex. We propose that in the *Rab8* mutant, the increase of plasma membrane Ihog (mostly observed at the lateral membrane) leads to an entrapment of Hh at the lateral membrane of *P* cells leading to the increase of Hh basolaterally (Fig. 4G′) and enhancing the activation of the short-range targets. These data also show that endocytosed Hh molecules are likely not regulated similarly, as only half of the endosomes containing Hh contain both Hh and Ihog. In addition, Hh internalization to $Rab5^{CA}$-YFP endosomes is only very slightly modulated by Rab8, but those endosomes tend to localize more towards the lateral side of *P* cells. This could also contribute to the increase of lateral Hh distribution in *P* cells.

Rab8 is required to maintain a low level of Ihog at the plasma membrane, which is necessary for proper Hh target activation

We then questioned whether the accumulation of Ihog alone at the plasma membrane observed in *Rab8*-depleted cells is the cause of the strong *Rab8* mutant phenotype, namely an increased expression of Hh short-range targets and a decrease of its long-range targets. To test this, we lowered Ihog levels in *P* cells of $Rab8^{U1}$ mutant discs and investigated whether this would restore normal Hh distribution and expression of both long- and short-range targets of Hh. Strikingly, inducing *ihog* RNAi was sufficient to restore the expression of proximal Hh targets close to wild-type levels, with a decrease of En and Ptc expansion and an increase of proximal *dpp* but not of distal *dpp* (Fig. 8A-F) suggesting that Hh could still have impaired apical release. To further analyse this, we have quantified the distribution of extracellular Hh in *P* cells in which both *ihog* and *Rab8* are removed. We depleted *ihog* in the dorsal compartment of $Rab8^{U1}$ mutant discs, and quantified extracellular Hh in both the dorsal and the ventral compartments section by section. We observed a reduction in the level of both apical and lateral ExHh distribution, with the lateral ExHh showing the strongest reduction (reduced by almost 50%; Fig. 8G-H). This correlates with the rescue of the short-range target En in *A* cells. Normal apical Hh release is probably not rescued because Rab5 endosomes are still mislocalized in this context (Fig. 8I-I‴). It also suggests that the mislocalization of Rab5 endosomes in the $Rab8^{U1}$ mutant is independent of Ihog.

This result shows that Rab8 is required to maintain a low level of Ihog at the lateral membrane by promoting its internalization. When Rab8 is absent, Ihog accumulates at the lateral plasma membrane and traps Hh, which activates its short-range targets more than in wild type.

DISCUSSION

Here, we identified Rab8 as a regulator of the Hh gradient. We first show that depletion of *Rab8* differentially affects the expression of Hh target genes. Short-range target expression is expanded whereas long-range target expression is decreased. We show that the *Rab8* mutant phenotype is not only due to an increase of released Hh at the lateral side of producing cells but also to a simultaneous reduction of Hh released apically. We conclude that Rab8 influences the formation of the functional Hh gradient that is directly linked to a controlled balance between the apical and basolateral pools of Hh.

Rab8 loss of function induces Hh short-range target expression by promoting the lateral release of Hh

The wild-type Hh gradient in the wing imaginal disc leads to the activation of long (*dpp*) and short-range (En, Ptc) target gene expression. In parallel, the Hh gradient is established by Hh apical and basolateral release from *P* cells followed by its spreading. However, the link between apical/basolateral release and spreading, and the short/long-range target activation is not clear. A number of studies link apical release and spreading to long-range target activation, whereas basolateral release is linked to short-range effects. For instance, we have previously shown that an increase of apical Hh level, by expressing a secreted form of the glypican Dally, promotes Hh long-range activity (Ayers et al., 2010). However, other studies contradict this, and suggest that Hh-enriched long filopodia formation from the basolateral membrane activates long-range targets (Bilioni et al., 2013; Bischoff et al., 2013; Callejo et al., 2011; Chen et al., 2017).

Here, we show that the loss of *Rab8* leads to a change in Hh target activation: in absence of *Rab8*, released lateral Hh accumulates in receiving *A* cells (Fig. 4), leading to the expansion of Ptc and En expression (short-range targets that are both known to respond to high-level signalling). Importantly, we show that reducing the overall Hh level in the *Rab8* mutant suppresses this expansion (Fig. 3I-K). Taken together, these data suggest that the high level of Hh signalling that promotes short-range target expression is controlled by the lateral pool of Hh.

Rab8 loss of function induces a decrease in long-range target expression and mispositioning of apical early Rab5 endosomes

Conversely, Rab8 loss of function also leads to reduced long-range target expression, which has been linked to Hh apical release (Figs 2 and 3). Interestingly, we found less apical released Hh at the surface of receiving *A* cells in *Rab8* mutant discs, whereas Hh accumulates apically in *P* producing cells (Fig. 4). In wild type, the apical secretion of newly synthesized Hh in *P* cells is followed by Hh internalization to apical Rab5 endosomes. From there, it has been proposed that Hh is then quickly recycled to the apical membrane from where it is released to promote long-range target expression (D'Angelo et al., 2015). Consistent with this, we observed the resulting decrease in *dpp* expression (which is known to respond to low-level signalling) upon blocking apical Hh endocytosis in producing cells (Ayers et al., 2010).

Development (2021) 148, dev191791. doi:10.1242/dev.191791

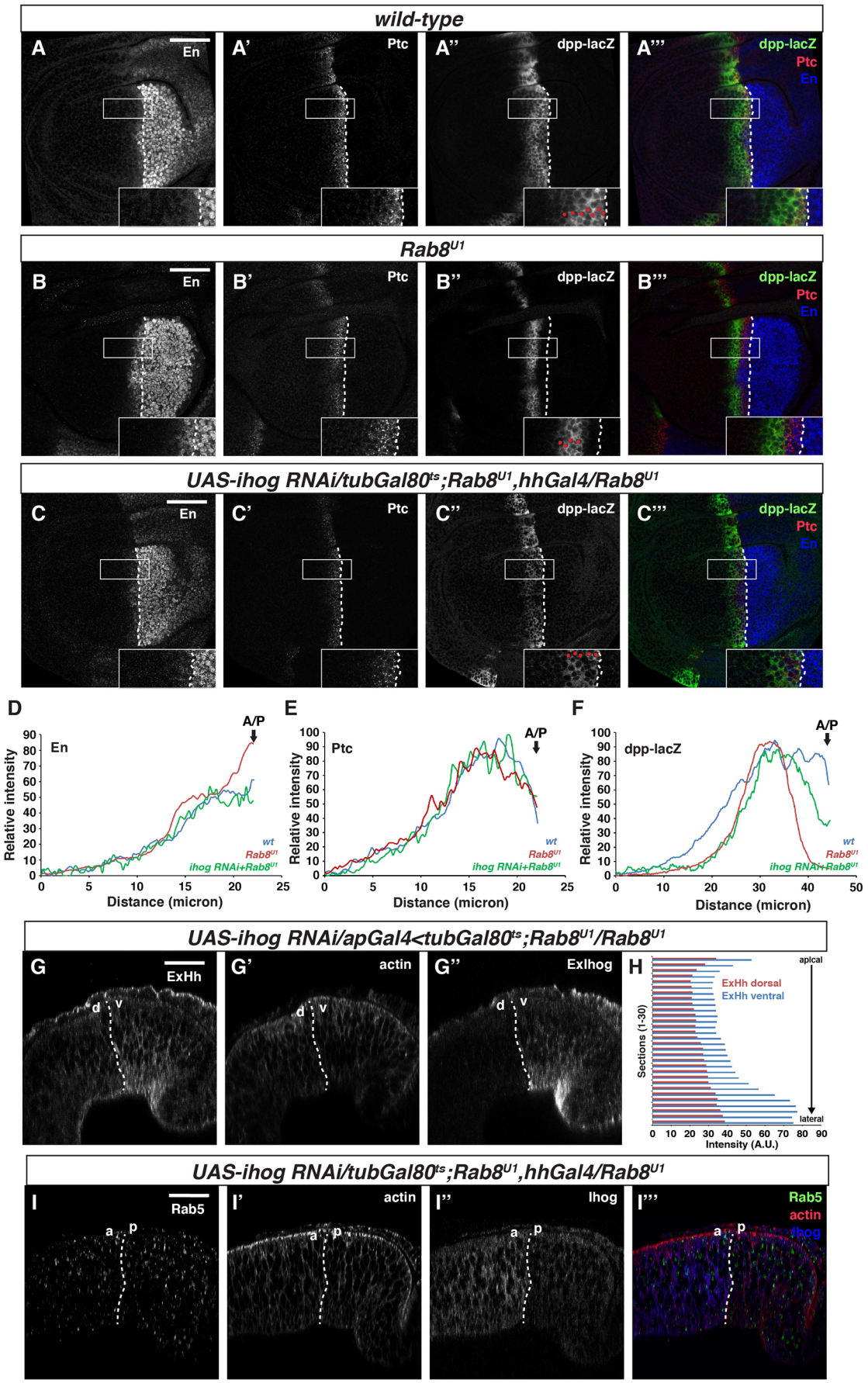

Fig. 8. See next page for legend.

Development (2021) 148, dev191791. doi:10.1242/dev.191791

Fig. 8. Depletion of Ihog in *Rab8* mutant *P* cells partially rescues Hh target gene expression but not Rab5 distribution. (A-B‴) Wild-type (A-A‴) and $Rab8^{U1}$ mutant (B-B‴) discs stained with En, Ptc and β-gal. (C-C‴) Overexpression of *ihog* dsRNA in *P* cells of $Rab8^{U1}$ mutant. In all *xy* confocal images dorsal is up, and posterior is to the right. (D-F) Quantification of En, Ptc and *dpp-lacZ* in the aforementioned genotypes. The A/P boundary is indicated by a black arrow. (G-G″) Single *z*-sections along the posterior compartment in discs overexpressing *ihog* dsRNA in the dorsal compartment in a $Rab8^{U1}$ mutant, stained for extracellular Hh (ExHh), actin and extracellular Ihog (ExIhog). The white dashed lines mark the dorsoventral border. d, dorsal; v, ventral. (H) Section by section quantification of extracellular Hh labelling in the genotype shown in G-G″. (I-I‴) Single *z*-section along the *P* compartment of discs overexpressing *ihog* dsRNA in the *P* compartment in a $Rab8^{U1}$ mutant, stained for Rab5, actin and Ihog. a, anterior; p, posterior. Red dots indicate cells expressing *dpp-lacZ*. Scale bars: 50 µm.

However, Rab8 is not essential for Hh endocytosis. Instead, it modulates the positioning of the endosomes in which Hh is internalized. Indeed, in the *Rab8* mutant, instead of being apical, these early endosomes are more lateral. As the trafficking of Hh through Rab5 endosomes is instrumental for its long-range target expression (D'Angelo et al., 2015), the lateral shift of these endosomes could potentially contribute to the decrease of distal *dpp* expression. Furthermore, with these endosomes now more lateral, more Hh may be recycled to the basolateral membrane, thus contributing to the increase of short-range target expression.

We propose that the mispositioning of the early endosomes through which apical Hh is normally recycled decreases Hh recycling to the apical membrane and possibly increases its recycling to the basolateral membrane. Taken together, our data also suggest that the low level of Hh signalling that promotes long-range target expression is controlled by the apical pool of Hh.

Rab8 controls Ihog endocytosis

The second *Rab8* loss-of-function phenotype observed is the accumulation of the Hh co-receptor Ihog at the lateral membrane. Interestingly, Rab8 and Ihog co-precipitate. Whether they bind directly and whether the Ihog binding depends on the Rab8 GTP/GDP loading is not known but it opens the possibility that Ihog is a novel Rab8 effector.

A model for regulation of the Hh gradient by Rab8

To explain the phenotype observed with *Rab8* loss of function, we propose the following model: Ihog that accumulates at the basolateral membrane would associate with Hh and keep it close to the source, in order to present the lateral Hh to its receptor in *A* cells in such a way that its high concentration would activate short-range targets. In support of this model, Ihog depletion in the posterior compartment in the $Rab8^{U1}$ mutant context is sufficient to restore the wild-type expression of the Hh short-range targets because Ihog is less accumulated (Fig. 8).

We propose that the mislocalization of the early Hh-containing endosomes to a more basolateral position (Fig. 7) enhances Hh recycling to the basolateral membrane where it would be trapped further by a high level of Ihog (thus promoting short-range target activation). Furthermore, the phenotypic consequence of the endosome mispositioning might be greater than this, and may influence Hh signalling beyond Ihog. Importantly, the mispositioning of the early endosomes observed with *Rab8* loss of function is not linked to Ihog accumulation, as Ihog overexpression in *P* cells does not lead to endosome mispositioning (Fig. S6M-M″) and depleting Ihog did not rescue endosomal mispositioning in the *Rab8* mutant (Fig. 8). In other words, the position of early endosomes depends on Rab8, not Ihog.

Taken together, the *Rab8* mutant phenotype can be explained by (1) trafficking of Hh into abnormally mislocalized Rab5 endosomes, and (2) the abnormal accumulation of Ihog predominantly at the lateral membrane due to its impaired endocytosis.

Our understanding of the establishment of the Hh extracellular gradient

Two pools of Hh to form one gradient

Our data confirm that the Hh gradient is composed of a combination of apical and basolateral Hh pools resulting from the release of Hh at the two membrane sites. Evidence that the apical Hh pool is not equivalent to the basolateral pool is also illustrated by the production of Hh by photoreceptor neurons in the developmental eye disc (Huang and Kunes, 1996). There, Hh is apically released to control propagation of the ommatidial differentiation, and basally released along photoreceptor axons to regulate cell division. Production of two different pools might be important for the association of Hh to a carrier that will participate differently in its release, spreading and activity.

Interestingly, we have previously often observed a trade-off between the long- and short-range Hh pathway targets upon modification of Hh trafficking in *P* cells (Ayers et al., 2010). Indeed, a simultaneous increase in expression of the long-range target *dpp* and a decrease in that of the short-range target En target were observed upon blocking of apical Hh endocytosis, suggesting that the apical and basolateral Hh pools responsible for the differential target activation are not independent (Ayers et al., 2010). In the present study, we provide an additional example in which this trade-off is observed: the depletion of *Rab8* differentially affects the expression of Hh target genes with expansion of the short-range target En and a simultaneous decrease in the long-range target *dpp*. This confirms that there is an active cellular machinery in place for the controlled balance between apical and basolateral Hh release and gradient formation.

Our data show that endocytosed Hh in Rab5 endosomes exists as two separated pools. The first is an Ihog-independent pool that does not appear to meet Ihog in the early endocytic compartment. The second is a pool of Hh that is present with Ihog in early endosomes. It is thus possible that, depending on the interactors on which Hh binds at the apical plasma membrane after initial secretion, the routing of endocytosed Hh differs. The presence of Ihog and Hh in common endocytic structures suggests that Ihog could participate in directing endocytosed Hh to another subcellular compartment or plasma membrane domain. It is likely that Ihog/Hh interaction would lead to a differential recycling instead of degradation as we did not find any evidence for Ihog (Fig. S7) or Hh (D'Angelo et al., 2015) trafficking to a degradative compartment. The formation of these two Hh pools might require specific sorting and targeting machineries that are distinct but also somehow connected to allow the trade-off mentioned earlier. We propose that some Hh could be recycled without Ihog in producing cells from apical to apical location or transcytose with Ihog from the apical to the lateral or basal pole.

In conclusion, our observations from *Rab8* loss of function are consistent with the existence of two pools of Hh that contribute differently to its functional extracellular gradient. This illustrates the probable influence of intracellular trafficking on the routes followed directly or indirectly by Hh and on the genesis of different Hh pools in the columnar epithelial cells.

MATERIALS AND METHODS

Drosophila culture and genetics

Flies were raised on standard *Drosophila* medium. w^{1118} was used as wild-type control in all experiments. Rescue experiments for $Rab8^{U1}$ were

Development (2021) 148, dev191791. doi:10.1242/dev.191791

performed by making a stable line expressing Rab8-CFP (genomic rescue construct, kindly provided by M. Brankatschk and S. Eaton, Max Planck Institute of Molecular Cell Biology and Genetics, Germany) with *Rab8^{U1}*, or by combining *UAS-Rab8-YFP* (Bloomington *Drosophila* Stock Center, BL#9782) with *armGal4* in a *Rab8^{U1}* homozygous background at 25°C. All experiments were repeated at least three times.

In the rescue experiments of Hh-dependent wing imaginal disc outgrowth, 15 virgins of the 'tester line', *w^{1118}; tubGal80^{ts}; hhGal4<UAS-Hh(M4)/TM6b,Tb* (Matusek et al., 2014), were crossed to five males of control RNAi lines (see below) and *Rab8* alleles [*UAS-Rab8^{28092GD}*: Vienna *Drosophila* Resource Center, VDRC#28092, *Rab8^{pBacB229}*: BL#16174, *Df(3L)BSC445*: BL#2494] in each vial. Flies were transferred to new vials every 6-8 h at 25°C to allow sufficient egg laying and avoid overcrowding. Vials containing early 2nd instar larvae were shifted to 29°C to inactivate *tubGal80^{ts}* thus activating *UAS-Hh(M4)* expression and the UAS transgenes tested in the system. After 3 days of incubation at 29°C wandering 3rd instar larvae were dissected and their phenotype scored in a double-blind manner (Fig. 1). *UAS-ci^{105620KK}* (VDRC#100620) and *UAS-disp^{10004GD}* (VDRC#10004) RNAis, as well as *dpp^{d12}* (BL#2070), *dpp^{d14}* (BL#3555) (*dpp* loss-of-function alleles), *tkv^{7}* (BL#3242) and *tkv^{8}* (BL#34509) (*dpp* receptor *thick-vein* loss-of-function alleles) were used as controls.

To monitor Hh target gene expression patterns in the Hh gain-of-function context *w^{1118}; tubGal80^{ts}<dpp-lacZ; hhGal4<UAS-Hh(M4)/TM6b,Tb* virgins were crossed to *w^{1118}* and *UAS-Rab8^{28092GD}*, respectively. Crosses were raised as described above for the wing disc morphology rescue assay (Fig. 1).

To induce a strong loss of function of *Rab8* specifically in the posterior compartment, we made use of *Rab8^{EYFP}* (kindly provided by S. Eaton and M. Brankatschk before publication, currently available as BL#62546) line, in which YFP^{MYC} tag is inserted in the N terminus of *Rab8* using homologous recombination (Dunst et al., 2015). *y^{1},w^{1118}; UAS-Rab8^{28092GD}; Rab8^{EYFP}/SM6-TM6b* flies were crossed to *UAS-deGradFP; hhGal4/SM6-TM6b.* In these animals, *hhGal4* drives the expression of *UAS-deGradFP* (BL#38422), which degrades the YFP-tagged Rab8 protein. The untagged *Rab8* copy is simultaneously knocked down by *UAS-Rab8^{28092GD}* RNAi giving rise to a strong hypomorphic condition. For these experiments, egg laying was performed at 25°C and vials were then shifted up to 29°C (Fig. 2; Figs S1 and S2).

In order to generate new loss-of-function alleles of *Rab8*, we remobilized a P-element positioned upstream of the *Rab8* locus, *w^{1118}; P{RS3}CB-5247-3* (*Drosophila* Genetic Resource Center, DGRC#123526) (Fig. S1). We recovered four putative *Rab8* alleles that showed pupal lethality over the overlapping *Df(3L)BSC445* deficiency. Three exhibited a recessive, mid/brown pupal lethal phase whereas the fourth showed pharate adult pupal lethality in homozygous conditions and also over the overlapping deficiency *Df(3L)BSC445*. This latter late lethal phenotype was consistent with the previously published lethal phase of *Rab8* transallelic mutant combinations (West et al., 2015), implying that this imprecise excision was probably a novel, amorphic *Rab8* allele. To confirm this, we mapped the deficiency breakpoints of this excision, which deleted 258 bp from the *Rab8* locus, including part of the 5′ UTR and the first exon, without affecting the neighbouring *CG8334* locus. To rescue the lethal phenotype, we reintroduced *UAS-Rab8-YFP* (BL#9782) to the homozygous mutant background using the general *armGal4* (BL# 1560) driver, which showed a partial rescue of the lethal phenotype, and reintroduction of a single ectopic genomic copy of the *Rab8* locus completely restored viability. We therefore concluded that the 258 bp excision we mapped, and named as *Rab8^{U1}*, in the *Rab8* locus is indeed a clean, novel *Rab8* allele, and no other essential loci are affected.

For compartment-specific *Rab8* knockdown experiments, *UAS-Rab8^{28092GD};UAS-Dcr2/ SM6-TM6b* males were crossed to *ptcGal4<dpp-lacZ* or *apGal4;+/ SM6-TM6b* virgins. Crosses were raised at 29°C until dissection (Fig. S1).

For compartment-specific *Rab8* rescue experiments, *UAS-Rab8-YFP; Rab8^{U1}/SM6-TM6b* males were crossed to *ptcGal4<dpp-lacZ;Rab8^{U1}/TM6b* and *dpp-lacZ;hhGal4<Rab8^{U1}/TM6b,Tb* virgins, respectively. Crosses were raised at 25°C until dissection (Fig. S1).

To establish a sensitized background with low anterior En expression, we generated a hypomorphic *hh* condition by crossing *y^{1},w^{1118}; Rab8^{28092GD}; hh^{ts2}/ SM6-TM6b* with *y^{1},w^{1118}; dpp-nuc-lacZ^{P10638}; hhGal4/ SM6-TM6b*. *dpp-nuc-lacZ^{P10638}* was kindly provided by L. Xinhua (State Key Laboratory of Genetic Engineering, Fudan University, China). *hh^{ts2}* (BL#1684) is a temperature-sensitive, conditional null allele of *hh* and *hhGal4* is an enhancer trap line (Tanimoto et al., 2000), and is itself a weak hypomorph. The heteroallelic combination of *hh^{ts2}/hhGal4* therefore behaves as a *hh* hypomorph when kept at 29°C. For the experiments, egg laying was carried out at 18°C and vials were shifted to 29°C in the 1st instar stage. Similarly, to reduce the amount of Hh in *Rab8^{U1}* homozygotes, *w^{1118}; hh^{ts2}<Rab8^{U1}/TM6b,Tb* males were crossed to *w^{1118}; dpp-lacZ;Rab8^{U1}/TM6b,Tb* virgins, and early 1st instar larvae were shifted to 29°C until dissection (Fig. 3).

To trap secreted Hh in the anterior cells, *UAS-ptc^{1130X}* (BL#44612) and *UAS-ptc^{1130X}; Rab8^{U1}/TM6b,Tb* males were crossed with *ptcGal4<tubGal80^{ts}* and *ptcGal4<tubGal80^{ts}; Rab8^{U1}/TM6b,Tb* virgins, respectively. The crosses were kept at 18°C until larvae reached the wandering stage. Ptc^{1130X} expression was induced either continuously, or for 4 h at 29°C. This condition allows the spreading of Hh in the receiving tissue and captures the extent of the Hh gradient along the Ptc domain (Fig. 4; Fig. S4).

To obtain a strong hypomorphic condition of *Rab8* in the dorsal compartment, the *y^{1},w^{1118}; Rab8^{28092GD}; Rab8^{EYFP}/SM6-TM6b* line was crossed to *w^{1118}; apGal4<dpp-nuc-lacZ^{P10638}/CyO; UAS-GFP-RNAi<UAS-deGradFP/TM6b,Tb*. Crosses were maintained at 25°C. In this context, Rab8^{EYFP} from one chromosome is suppressed by three mechanisms (*deGradFP*, *GFP* RNAi and *Rab8* RNAi; Fig. 5; Fig. S5) and untagged Rab8 is depleted by *Rab8* RNAi.

Temporally controlled overexpression of *UAS-IhogRFP* (kindly provided by I. Guerrero; Callejo et al., 2011) in the control or *Rab8^{U1}* mutant background was induced by crossing *UAS-IhogRFP<tubGal80^{ts}; hhGal4<Rab8^{U1}/TM6b,Tb* males to *Rab8^{U1}/TM6c,Tb,Sb* virgins. Crosses were kept at 18°C and flipped every day. Early 3rd instar larvae were shifted at age 168 h at 18°C to 29°C for 24 h and then incubated at 18°C again for 72 h (Fig. 5). To detect if Rab5 endosome mislocalization can be induced by increased Ihog levels, IhogRFP overexpression in wild-type background was induced by crossing *tubGal80^{ts}<Rab5^{KI}; hhGal4 /TM6b,Tb* virgins to *UAS-IhogRFP* males. Early third instar larvae were shifted to 29°C for 24 h before dissection (Fig. S6).

To monitor the accumulation of Hh, Ihog and Rab8 in early endosomes (Figs 6 and 7; Fig. S6), *UAS-Rab5^{CA}-YFP* (BL#9774) or *UAS-Rab5^{CA}-YFP; Rab8^{U1}/TM6c,Tb,Sb* virgins were crossed to *y^{1},w^{1118}; tubGal80^{ts}<dpp-nuc-lacZ^{P10638};hhGal4/ SM6-TM6b*, or *y^{1},w^{1118}; apGal4<tubGal80^{ts};+/SM6-TM6b* and *y^{1},w^{1118};tubGal80^{ts}<dpp-nuc-lacZ^{P10638};hhGal4<Rab8^{U1}/SM6-TM6b*, respectively. Crosses were kept at 18°C. The expression of Rab5^{CA}-YFP was induced for 16-17 h prior to dissection by shifting vials containing early 3rd instar larvae to 29°C.

To monitor the mislocalization of endogenous Rab5 endosomes, Rab5^{EGFP} knock-in (Rab5^{KI}; Fabrowski et al., 2013) was introduced to the *Rab8^{U1}* background. *Rab5^{KI}/CyO* control and *Rab5^{KI}/CyO;Rab8^{U1}/TM6b,Tb* males were crossed to *w^{1118}* and *Rab8^{U1}/TM6c,Tb,Sb* virgins, respectively. Crosses were raised at 25°C, and larvae were dissected at L3 stage (Fig. S6).

ihog RNAi (VDRC#29897) expression was induced by crossing *UAS-ihog^{GD29897}; Rab8^{U1}/SM6-TM6b* males to *tubGal80^{ts}<dpp-lacZ; hhGal4<Rab8^{U1}/TM6b,Tb* or *apGal4<tubGal80^{ts}; Rab8^{U1}/TM6b,Tb* virgins. First instar larvae were shifted to 29°C until dissection (Fig. 8). Vps4^{DN} overexpression was induced for 6 h as described previously (Matusek et al., 2014). *dor* loss-of-function clones were generated as described previously (D'Angelo et al., 2015.)

DNA extraction, PCR and sequencing of *Rab8^{U1}*

Genomic DNA was isolated from *Rab8^{U1}* homozygous mutant larvae using a standard protocol (DNeasy Blood & Tissue Kit) and PCR was performed using the following primer pairs: (1) 5′ GTAATTTTCACAACAAACCA-ACGTAG, 3′ AAAAGAGGCATTTAATGAGTCACTG; (2) 5′ GTAAT-TTTCACAACAAACCAACGTAG, 3′ CGAAAATAAACAATTATTAGC-CACGAG.

The PCR product was cut from the gel and was purified using a Qiagen gel purification kit (28706). The sample was sequenced by Eurofins and breakpoints were mapped using multiple sequence alignment by ClustalW.

Development (2021) 148, dev191791. doi:10.1242/dev.191791

Immunostaining

Conventional and extracellular (without fixation and detergent at 4°C) immunolabelling was performed as previously described (Matusek et al., 2014). For extracellular labelling without detergent but with initial fixation, we used the protocol described by D'Angelo et al. (2015). Briefly, discs were dissected in ice-cold PBS, and then fixed in 2% paraformaldehyde in PBS for 15 min at room temperature. After fixation, discs were rinsed in PBS three times for 5 min at room temperature, and then incubated with anti-Hh antibody (1/400) for 1 h in 2% BSA in PBS. For imaging, wing imaginal discs were mounted in VECTASHIELD mounting medium (Vector Laboratories).

Primary antibodies

Antibodies used were as follows: rabbit anti-Rab5 (1/150, Abcam, ab31261); rabbit anti-En (1/1000, Santa Cruz Biotechnology, sc-28640); mouse anti-Ptc [1/400, provided by P. Ingham, Lee Kong Chian (LKC) School of Medicine at Nanyang Technological University, Singapore]; chicken polyclonal anti-β-gal (1/1000, GeneTex, GTX77365); affinity-purified rabbit anti-Hh (1/500) and rabbit anti-Hh (preadsorbed) (1/500) (Gallet et al., 2003; Matusek et al., 2014); mouse anti-hRab8 (1/200, BD Biosciences, 610844); anti-tubulin (used for the western blot; 1/10,000, GeneTex, GTX100117); mouse anti-GFP (1/100, Roche, 1814460); rat anti-DE-Cadherin (1/50, DSHB, DCAD2); mouse anti-Dlg (1/50, DSHB, 4F3); rabbit anti-Caspase-III (1/500, Cell Signaling Technology, 9661); rabbit anti-aPKC (1/500, Santa Cruz Biotechnology, sc-216); rat polyclonal anti-Ihog (1:100, generated in this study); mouse anti-FasIII (1/100, DSHB, 7G10); mouse anti-Armadillo (1/100, DSHB, N2 7A1), guinea pig anti-HRS antibody (1/500, provided by Hugo Bellen, Howard Hughes Medical Institute, Baylor College of Medicine, Texas, USA); mouse-anti-Ubi (1/1000, clone FK2, ENZO Life Sciences, BML-PW8810-0100).

Generation of the antibody against Ihog

The Ihog coding sequence from amino acids 1 to 486 was cloned into pGetStablyA vector in phase with 6his tag at the C terminal.

E. coli SE1 strain was used for recombinant protein production (Eurogenetec). Ni-NTA affinity resin (Qiagen) was used for the His6-tagged Ihog purification by standard protocol under denaturing conditions. Two rats were immunized, and blood samples were analyzed after several boosts. Validation of the serum used in this study was performed on imaginal disc depleted for Ihog (see Fig. 8G″,I″).

Secondary antibodies

Fluorescent secondary antibodies used were as follows: goat anti-rabbit Alexa 488 (1/500, Life Technologies, A11008); goat anti-rabbit DyLight649 (1/500, Jackson ImmunoResearch Laboratories, 211-492-171); goat anti-rabbit Cy5 (1/200, Jackson ImmunoResearch Laboratories, 111-175-144); goat anti-mouse Alexa 488 (1/500, Life Technologies, A32723); donkey anti-mouse Alexa 546 (1/500, Life Technologies, A10036); Cy5-conjugated donkey anti-rat (1/200, Jackson ImmunoResearch Laboratories, 712-175-150); Cy3- or FITC-conjugated donkey anti-chicken (1/200, Jackson ImmunoResearch Laboratories, 703-165-155, 703-095-155); Cy3-conjugated anti-guinea pig (1/200, Jackson ImmunoResearch Laboratories, 106-165-003); Rhodamine phalloidin (1/100, Sigma-Aldrich, P1951).

Immunoprecipitation (IP) and western blot (WB) analyses from S2R+ cells

For IP and WB analyses, cells were lysed in lysis buffer (20 mM TrisHCl-pH 8, 150 mM NaCl and 1% Triton X-100) in the presence of phosphatase inhibitors (50 mM sodium fluoride and 10 mM sodium orthovanadate) and protease inhibitors 2 days after transfection. HA-tagged proteins (Fig. 6) were precipitated with a mouse anti-HA antibody (12CA5, Sigma-Aldrich) and immunocomplexes were resolved by SDS-PAGE. WBs were performed three times with antibodies against Hh and HA as described previously (Ranieri et al., 2012). Rab8 protein was detected with a mouse anti-hRab8 (BD Biosciences, 610884) and Ihog protein with a rat anti-Ihog antibody (generated in house).

WB analyses from larvae

For WB analyses (Figs S1 and S3), 20 larvae were homogenized in 300 µl cold RIPA buffer (50 mM Tris-pH 8, 150 mM NaCl, 1% NP40, 0.1% SDS and 0.1% deoxycholic acid) in the presence of phosphatase inhibitors (50 mM sodium fluoride and 10 nM sodium orthovanadate) and protease inhibitors. Protein levels were determined using the Bio-Rad Protein Assay (Bio-Rad Laboratories). Approximately 20 µg of proteins were used for WB. Lysates were analysed using anti-Hh, anti-hRab8 and anti-Armadillo as previously described (Ruel et al., 2007). WBs were performed three times.

Cell culture, transfections and DNA constructs

Drosophila Schneider line-2R+ (S2R+) cells were maintained as described by Ruel et al. (2007). The following constructs were described previously (Zheng et al., 2010): Ihog-HA, IhogΔCTD-HA, IhogΔFN1-HA, IhogΔFN2-HA. For Rab8, *UASp-Rab8-YFP* was described by Zhang et al. (2007).

RNA interference in S2R+ cells and luciferase assay

Double-stranded RNAs were produced by *in vitro* transcription of a PCR product corresponding to the coding sequence (nucleotide position 84-274) of *Rab8*. Transfection of S2 cells with dsRNA was carried out following the protocol described by Clemens et al. (2000). After 1 day of incubation with dsRNA, 2 µg of *actin*-Hh-*Renilla* (in which the coding sequence for *Renilla* luciferase was inserted into the N-terminal signalling domain of Hh; Aikin et al., 2012) and 2 µg of *actin*-Firefly (to normalize for transfection efficiency) were transfected and incubated during 48 h. The supernatants (from cells treated with *Rab8* RNAi and control) were then analysed by WB, and for *Renilla* activity (Fig. S3). The same cells were prepared for WB analysis. *Renilla* and Firefly activity was measured with Luciferase Assay Kits (Promega). This experiment was performed three times.

Imaging and image analysis

A Leica SP5 confocal microscope was used for imaging. Captured images were analysed using Fiji software and Adobe Photoshop CS5. Most of the images show single 1 µm sections unless stated otherwise from apical, sub-apical and lateral planes of the disc. *Z*-sections were taken at 500 nm or 1 µm thickness. Intensity plot analysis was carried out in Fiji and *xy* coordinate values were exported to Microsoft Excel for plotting. En and Ptc anterior intensities were quantified using the Fiji 'Measure' command in 25×50 pixel rectangles on 3 µm stack volumes at the anterior-posterior (A/P) boundary for Fig. 3.

Ihog immunolabelling intensities (Fig. S5) were quantified using the same command in a 50×50 pixel square for single *xy*-sections and 50×100 pixel rectangles on single confocal *z*-sections.

Ihog and extracellular Hh apicobasal distribution and immunofluorescence intensity was measured on single *xy* sections, slice by slice using 50×50 pixel squares. Obtained values were exported and plotted in Microsoft Excel (Figs. 4, 5 and 8).

Ihog- and Hh-containing $Rab5^{CA}$-YFP vesicle counting was performed using the Fiji Cell counter plugin on reconstructed, 10-µm-thick *z*-volumes, in which 300 vesicles per disc were counted manually and the obtained vesicle numbers were exported to Microsoft Excel and the percentages plotted (Fig. S6L).

The distance between $Rab5^{CA}$-YFP and $Rab5^{KI}$ endosomes and the apical plasma membrane were measured manually on nine independent discs, using Cadherin as an apical marker on nine non-overlapping single *z*-sections per disc. First, the average thickness of the tissue was estimated by taking eight measurements along the whole columnar epithelium perpendicular to the apical membrane. Tissue thickness values were then averaged and normalized to 50 µm between discs to obtain comparable distribution values for $Rab5^{CA}$-YFP and $Rab5^{KI}$ variants and correct for variation of section thicknesses. Distances of $Rab5^{CA}$-YFP and $Rab5^{KI}$ endosomes from the apical marker were measured manually with Fiji, and the obtained values were then exported to Microsoft Excel. The percentage of endosomes present at different distances from the apical marker (where 0 stands for the apical marker level on the graphs) were plotted against distance intervals (Fig. 7; Fig. S6). *P*-values were calculated using unpaired two-tailed *t*-tests.

Acknowledgements
We thank all 'fly' members of the IBV Institute, and Gabor Hajnal-Papp for additional help. We also thank Julien Marcetteau, Olivier Devergne and Rolland Leborgne for discussion and/or critical analysis of the manuscript.

Competing interests
The authors declare no competing or financial interests.

Author contributions
Conceptualization: P.P.T., T.M.; Methodology: T.M.; Validation: P.P.T., T.M., T.G., G.D., C.G., L.L.-S.; Formal analysis: P.P.T., T.M., T.G., G.D., C.G.; Investigation: T.M., T.G., G.D., C.G., T.T., L.L.-S.; Resources: P.P.T.; Data curation: T.M.; Writing - original draft: P.P.T.; Writing - review & editing: P.P.T., T.M., C.R.; Supervision: P.P.T., T.M.; Project administration: P.P.T.; Funding acquisition: P.P.T.

Funding
T.G. held an AXA Research Fund and Fondation ARC pour la Recherche sur le Cancer fellowship, C.G. held a Fondation ARC pour la Recherche sur le Cancer fellowship. This work was supported by grants from Ligue Contre le Cancer 'Equipe labellisée 2016', the LABEX SIGNALIFE (ANR-11-LABX-0028-01) and the Agence Nationale de la Recherche (ANR-15-CE13-0002-01) to P.P.T.

Supplementary information
Supplementary information available online at
https://dev.biologists.org/lookup/doi/10.1242/dev.191791.supplemental

Peer review history
The peer review history is available online at
https://dev.biologists.org/lookup/doi/10.1242/dev.191791.reviewer-comments.pdf

References

Aikin, R., Cervantes, A., D'Angelo, G., Ruel, L., Lacas-Gervais, S., Schaub, S. and Thérond, P. (2012). A genome-wide RNAi screen identifies regulators of cholesterol-modified hedgehog secretion in Drosophila. *PLoS ONE* **7**, e33665. doi:10.1371/journal.pone.0033665

Ang, A. L., Fölsch, H., Koivisto, U.-M., Pypaert, M. and Mellman, I. (2003). The Rab8 GTPase selectively regulates AP-1B-dependent basolateral transport in polarized Madin-Darby canine kidney cells. *J. Cell Biol.* **163**, 339-350. doi:10.1083/jcb.200307046

Ayers, K. L., Gallet, A., Staccini-Lavenant, L. and Thérond, P. P. (2010). The long-range activity of Hedgehog is regulated in the apical extracellular space by the glypican Dally and the hydrolase Notum. *Dev. Cell* **18**, 605-620. doi:10.1016/j.devcel.2010.02.015

Babst, M., Sato, T. K., Banta, L. M. and Emr, S. D. (1997). Endosomal transport function in yeast requires a novel AAA-type ATPase, Vps4. *EMBO J.* **16**, 1820-1831. doi:10.1093/emboj/16.8.1820

Bellec, K., Gicquel, I. and Le Borgne, R. (2018). Stratum recruits Rab8 at Golgi exit sites to regulate the basolateral sorting of Notch and Sanpodo. *Development* **145**, dev163469. doi:10.1242/dev.163469

Bilioni, A., Sánchez-Hernández, D., Callejo, A., Gradilla, A.-C., Ibáñez, C., Mollica, E., Carmen Rodríguez-Navas, M., Simon, E. and Guerrero, I. (2013). Balancing Hedgehog, a retention and release equilibrium given by Dally, Ihog, Boi and shifted/DmWif. *Dev. Biol.* **376**, 198-212. doi:10.1016/j.ydbio.2012.12.013

Bischoff, M., Gradilla, A.-C., Seijo, I., Andrés, G., Rodríguez-Navas, C., González-Méndez, L. and Guerrero, I. (2013). Cytonemes are required for the establishment of a normal Hedgehog morphogen gradient in Drosophila epithelia. *Nat. Cell Biol.* **15**, 1269-1281. doi:10.1038/ncb2856

Burke, R., Nellen, D., Bellotto, M., Hafen, E., Senti, K.-A., Dickson, B. J. and Basler, K. (1999). Dispatched, a novel sterol-sensing domain protein dedicated to the release of cholesterol-modified hedgehog from signaling cells. *Cell* **99**, 803-815. doi:10.1016/S0092-8674(00)81677-3

Callejo, A., Bilioni, A., Mollica, E., Gorfinkiel, N., Andrés, G., Ibáñez, C., Torroja, C., Doglio, L., Sierra, J. and Guerrero, I. (2011). Dispatched mediates Hedgehog basolateral release to form the long-range morphogenetic gradient in the Drosophila wing disk epithelium. *Proc. Natl. Acad. Sci. USA* **108**, 12591-12598. doi:10.1073/pnas.1106881108

Capdevila, J. and Guerrero, I. (1994). Targeted expression of the signaling molecule decapentaplegic induces pattern duplications and growth alterations in Drosophila wings. *EMBO J.* **13**, 4459-4468. doi:10.1002/j.1460-2075.1994.tb06768.x

Caussinus, E., Kanca, O. and Affolter, M. (2012). Fluorescent fusion protein knockout mediated by anti-GFP nanobody. *Nat. Struct. Mol. Biol.* **19**, 117-121. doi:10.1038/nsmb.2180

Chen, Y. and Struhl, G. (1996). Dual roles for patched in sequestering and transducing Hedgehog. *Cell* **87**, 553-563. doi:10.1016/S0092-8674(00)81374-4

Chen, W., Huang, H., Hatori, R. and Kornberg, T. B. (2017). Essential basal cytonemes take up Hedgehog in the Drosophila wing imaginal disc. *Development* **144**, 3134-3144. doi:10.1242/dev.149856

Clemens, J. C., Worby, C. A., Simonson-Leff, N., Muda, M., Maehama, T., Hemmings, B. A. and Dixon, J. E. (2000). Use of double-stranded RNA interference in Drosophila cell lines to dissect signal transduction pathways. *Proc. Natl. Acad. Sci. USA* **97**, 6499-6503. doi:10.1073/pnas.110149597

D'Angelo, G., Matusek, T., Pizette, S. and Thérond, P. P. (2015). Endocytosis of Hedgehog through dispatched regulates long-range signaling. *Dev. Cell* **32**, 290-303. doi:10.1016/j.devcel.2014.12.004

Devergne, O., Sun, G. H. and Schüpbach, T. (2017). Stratum, a homolog of the human GEF Mss4, partnered with Rab8, controls the basal restriction of basement membrane proteins in epithelial cells. *Cell Rep.* **18**, 1831-1839. doi:10.1016/j.celrep.2017.02.002

Dunst, S., Kazimiers, T., von Zadow, F., Jambor, H., Sagner, A., Brankatschk, B., Mahmoud, A., Spannl, S., Tomancak, P., Eaton, S. et al. (2015). Endogenously tagged rab proteins: a resource to study membrane trafficking in Drosophila. *Dev. Cell* **33**, 351-365. doi:10.1016/j.devcel.2015.03.022

Fabrowski, P., Necakov, A. S., Mumbauer, S., Loeser, E., Reversi, A., Streichan, S., Briggs, J. A. G. and De Renzis, S. (2013). Tubular endocytosis drives remodelling of the apical surface during epithelial morphogenesis in Drosophila. *Nat. Commun.* **4**, 2244. doi:10.1038/ncomms3244

Fujita, H., Yamanaka, M., Imamura, K., Tanaka, Y., Nara, A., Yoshimori, T., Yokota, S. and Himeno, M. (2003). A dominant negative form of the AAA ATPase SKD1/VPS4 impairs membrane trafficking out of endosomal/lysosomal compartments: class E vps phenotype in mammalian cells. *J. Cell Sci.* **116**, 401-414. doi:10.1242/jcs.00213

Gallet, A., Rodriguez, R., Ruel, L. and Therond, P. P. (2003). Cholesterol modification of hedgehog is required for trafficking and movement, revealing an asymmetric cellular response to hedgehog. *Dev. Cell* **4**, 191-204. doi:10.1016/S1534-5807(03)00031-5

Gallet, A., Ruel, L., Staccini-Lavenant, L. and Thérond, P. P. (2006). Cholesterol modification is necessary for controlled planar long-range activity of Hedgehog in Drosophila epithelia. *Development* **133**, 407-418. doi:10.1242/dev.02212

González-Méndez, L., Seijo-Barandiarán, I. and Guerrero, I. (2017). Cytoneme-mediated cell-cell contacts for Hedgehog reception. *eLife* **6**, e24045. doi:10.7554/eLife.24045

Gradilla, A.-C., González, E., Seijo, I., Andrés, G., Bischoff, M., González-Mendez, L., Sánchez, V., Callejo, A., Ibáñez, C., Guerra, M. et al. (2014). Exosomes as Hedgehog carriers in cytoneme-mediated transport and secretion. *Nat. Commun.* **5**, 5649. doi:10.1038/ncomms6649

Guerrero, I. and Kornberg, T. B. (2014). Hedgehog and its circuitous journey from producing to target cells. *Semin. Cell Dev. Biol.* **33**, 52-62. doi:10.1016/j.semcdb.2014.06.016

Hattula, K., Furuhjelm, J., Tikkanen, J., Tanhuanpää, K., Laakkonen, P. and Peränen, J. (2006). Characterization of the Rab8-specific membrane traffic route linked to protrusion formation. *J. Cell Sci.* **119**, 4866-4877. doi:10.1242/jcs.03275

Henry, L. and Sheff, D. R. (2008). Rab8 regulates basolateral secretory, but not recycling, traffic at the recycling endosome. *Mol. Biol. Cell* **19**, 2059-2068. doi:10.1091/mbc.e07-09-0902

Huang, Z. and Kunes, S. (1996). Hedgehog, transmitted along retinal axons, triggers neurogenesis in the developing visual centers of the Drosophila Brain. *Cell* **86**, 411-422. doi:10.1016/S0092-8674(00)80114-2

Huber, L. A., Pimplikar, S., Parton, R. G., Virta, H., Zerial, M. and Simons, K. (1993). Rab8, a small GTPase involved in vesicular traffic between the TGN and the basolateral plasma membrane. *J. Cell Biol.* **123**, 35-45. doi:10.1083/jcb.123.1.35

Johnson, R. L., Milenkovic, L. and Scott, M. P. (2000). In vivo functions of the patched protein: requirement of the C terminus for target gene inactivation but not Hedgehog sequestration. *Mol. Cell* **6**, 467-478. doi:10.1016/S1097-2765(00)00045-9

Lum, L., Yao, S., Mozer, B., Rovescalli, A., Von Kessler, D., Nirenberg, M. and Beachy, P. A. (2003). Identification of Hedgehog pathway components by RNAi in Drosophila cultured cells. *Science* **299**, 2039-2045. doi:10.1126/science.1081403

Mann, R. K. and Beachy, P. A. (2004). Novel lipid modifications of secreted protein signals. *Annu. Rev. Biochem.* **73**, 891-923. doi:10.1146/annurev.biochem.73.011303.073933

Matusek, T., Wendler, F., Polès, S., Pizette, S., D'Angelo, G., Fürthauer, M. and Therond, P. P. (2014). The ESCRT machinery regulates the secretion and long-range activity of Hedgehog. *Nature* **516**, 99-103. doi:10.1038/nature13847

Mavor, L. M., Miao, H., Zuo, Z., Holly, R. M., Xie, Y., Loerke, D. and Blankenship, J. T. (2016). Rab8 directs furrow ingression and membrane addition during epithelial formation in Drosophila melanogaster. *Development* **143**, 892-903. doi:10.1242/dev.128876

Panáková, D., Sprong, H., Marois, E., Thiele, C. and Eaton, S. (2005). Lipoprotein particles are required for Hedgehog and Wingless signalling. *Nature* **435**, 58-65. doi:10.1038/nature03504

Parchure, A., Vyas, N., Ferguson, C., Parton, R. G. and Mayor, S. (2015). Oligomerization and endocytosis of Hedgehog is necessary for its efficient

exovesicular secretion. *Mol. Biol. Cell* **26**, 4700-4717. doi:10.1091/mbc.E15-09-0671

Pepinsky, R. B., Zeng, C., Wen, D., Rayhorn, P., Baker, D. P., Williams, K. P., Bixler, S. A., Ambrose, C. M., Garber, E. A., Miatkowski, K. et al. (1998). Identification of a palmitic acid-modified form of human Sonic hedgehog. *J. Biol. Chem.* **273**, 14037-14045. doi:10.1074/jbc.273.22.14037

Peränen, J. (2011). Rab8 GTPase as a regulator of cell shape. *Cytoskeleton (Hoboken)* **68**, 527-539. doi:10.1002/cm.20529

Ranieri, N., Ruel, L., Gallet, A., Raisin, S. and Thérond, P. P. (2012). Distinct phosphorylations on kinesin costal-2 mediate differential hedgehog signaling strength. *Dev. Cell* **22**, 279-294. doi:10.1016/j.devcel.2011.12.002

Ruel, L., Gallet, A., Raisin, S., Truchi, A., Staccini-Lavenant, L., Cervantes, A. and Thérond, P. P. (2007). Phosphorylation of the atypical kinesin Costal2 by the kinase Fused induces the partial disassembly of the Smoothened-Fused-Costal2-Cubitus interruptus complex in Hedgehog signalling. *Development* **134**, 3677-3689. doi:10.1242/dev.011577

Rusten, T. R., Vaccari, T., Lindmo, K., Rodahl, L. M. W., Nezis, I. P., Sem-Jacobsen, C., Wendler, F., Vincent, J.-P., Brech, A. et al. (2007). ESCRTs and Fab1 regulate distinct steps of autophagy. *Curr. Biol.* **17**, 1817-1825. doi:10.1016/j.cub.2007.09.032

Sanicola, M., Sekelsky, J., Elson, S. and Gelbart, W. M. (1995). Drawing a stripe in Drosophila imaginal disks: negative regulation of decapentaplegic and patched expression by engrailed. *Genetics* **139**, 745-756. doi:10.1093/genetics/139.2.745

Sato, T., Mushiake, S., Kato, Y., Sato, K., Sato, M., Takeda, N., Ozono, K., Miki, K., Kubo, Y., Tsuji, A. et al. (2007). The Rab8 GTPase regulates apical protein localization in intestinal cells. *Nature* **448**, 366-369. doi:10.1038/nature05929

Sato, T., Iwano, T., Kunii, M., Matsuda, S., Mizuguchi, R., Jung, Y., Hagiwara, H., Yoshihara, Y., Yuzaki, M., Harada, R. et al. (2014). Rab8a and Rab8b are essential for several apical transport pathways but insufficient for ciliogenesis. *J. Cell Sci.* **127**, 422-431. doi:10.1242/jcs.136903

Scales, S. J. and de Sauvage, F. J. (2009). Mechanisms of Hedgehog pathway activation in cancer and implications for therapy. *Trends Pharmacol. Sci.* **30**, 303-312. doi:10.1016/j.tips.2009.03.007

Sevrioukov, E. A., He, J. P., Moghrabi, N., Sunio, A., and Krämer, H. (1999). A role for the deep orange and carnation eye color genes in lysosomal delivery in Drosophila. *Mol. Cell* **4**, 479-486. doi:10.1016/s1097-2765(00)80199-9

Tanaka, Y., Okada, Y. and Hirokawa, N. (2005). FGF-induced vesicular release of Sonic hedgehog and retinoic acid in leftward nodal flow is critical for left–right determination. *Nature* **435**, 172-177. doi:10.1038/nature03494

Tanimoto, H., Itoh, S., ten Dijke, P. and Tabata, T. (2000). Hedgehog creates a gradient of DPP activity in Drosophila wing imaginal discs. *Mol. Cell* **5**, 59-71. doi:10.1016/S1097-2765(00)80403-7

Vervoort, M., Crozatier, M., Valle, D. and Vincent, A. (1999). The COE transcription factor Collier is a mediator of short-range Hedgehog-induced patterning of the Drosophila wing. *Curr. Biol. CB* **9**, 632-639. doi:10.1016/S0960-9822(99)80285-1

Vidal-Quadras, M., Holst, M. R., Francis, M. K., Larsson, E., Hachimi, M., Yau, W.-L., Peränen, J., Martín-Belmonte, F. and Lundmark, R. (2017). Endocytic turnover of Rab8 controls cell polarization. *J. Cell Sci.* **130**, 1147-1157.

Vyas, N., Walvekar, A., Tate, D., Lakshmanan, V., Bansal, D., Cicero, A. L., Raposo, G., Palakodeti, D. and Dhawan, J. (2014). Vertebrate Hedgehog is secreted on two types of extracellular vesicles with different signaling properties. *Sci. Rep.* **4**, 7357. doi:10.1038/srep07357

West, R. J. H., Lu, Y., Marie, B., Gao, F.-B. and Sweeney, S. T. (2015). Rab8, POSH, and TAK1 regulate synaptic growth in a Drosophila model of frontotemporal dementia. *J. Cell Biol.* **208**, 931-947. doi:10.1083/jcb.201404066

Yan, D., Wu, Y., Yang, Y., Belenkaya, T. Y., Tang, X. and Lin, X. (2010). The cell-surface proteins Dally-like and Ihog differentially regulate Hedgehog signaling strength and range during development. *Development* **137**, 2033-2044. doi:10.1242/dev.045740

Yao, S., Lum, L. and Beachy, P. (2006). The ihog cell-surface proteins bind Hedgehog and mediate pathway activation. *Cell* **125**, 343-357. doi:10.1016/j.cell.2006.02.040

Zeng, X., Goetz, J. A., Suber, L. M., Scott, W. J., Jr, Schreiner, C. M. and Robbins, D. J. (2001). A freely diffusible form of Sonic hedgehog mediates long-range signalling. *Nature* **411**, 716-720. doi:10.1038/35079648

Zhang, X. and Gao, N. (2016). RAB and RHO GTPases regulate intestinal crypt cell homeostasis and enterocyte function. *Small GTPases* **7**, 59-64. doi:10.1080/21541248.2016.1159274

Zhang, J., Schulze, K. L., Hiesinger, P. R., Suyama, K., Wang, S., Fish, M., Acar, M., Hoskins, R. A., Bellen, H. J. and Scott, M. P. (2007). Thirty-one flavors of Drosophila Rab proteins. *Genetics* **176**, 1307-1322. doi:10.1534/genetics.106.066761

Zheng, X., Mann, R. K., Sever, N. and Beachy, P. A. (2010). Genetic and biochemical definition of the Hedgehog receptor. *Genes Dev.* **24**, 57-71. doi:10.1101/gad.1870310